GRID-CONNECTED VARIABLE SPEED GENERATOR APPLICATIONS WITH DOUBLY-FED INDUCTION MACHINE

by
ERHAN DEMİROK

Submitted to the Graduate School of Engineering and Natural Sciences
in partial fulfillment of
the requirements for the degree of
Master of Science

Sabancı University
Summer 2007

GRID-CONNECTED VARIABLE SPEED GENERATOR APPLICATIONS WITH DOUBLY-FED INDUCTION MACHINE

APPROVED BY:

Prof. Dr. Asıf Şabanoviç …….

(Thesis Supervisor)

Assoc. Prof. Dr. Ahmet Onat …….

Assoc. Prof. Dr. Deniz Yıldırım …….

Assoc. Prof. Dr. Kemalettin Erbatur…….

Asst. Prof. Dr. Mahmut Akşit …….

DATE OF APPROVAL: …….

© Erhan Demirok 2007

All Rights Reserved

GRID-CONNECTED VARIABLE SPEED GENERATOR APPLICATIONS WITH DOUBLY-FED INDUCTION MACHINE

Erhan Demirok

EECS, MS Thesis, 2007

Thesis Supervisor: Prof. Dr. Asıf Şabanoviç

Keywords: Active and reactive power decoupling, generator, renewable energy, disturbance observer, doubly-fed induction machine, variable speed operation

Abstract

The thesis deals with power flow between grid and generator. Possible grid connection concepts are described and the topology of variable speed constant frequency with doubly-fed induction machine is emphasized among different topologies. The dynamical model and power flow analysis are realized to investigate the concept. In literature, the most preferred and implemented control method of doubly-fed induction generator, stator flux-oriented active-reactive power decoupling, is studied, simulated in the thesis and important drawbacks of the method are underlined. A nonlinear controller with disturbance observer is implemented to eliminate the drawbacks of flux-oriented based decoupling of active-reactive power. The proposed method brings in orientation-free and simple implementation to the concept. Stability analysis must be realized to satisfy exponential stability for controller performance and boundness of rotor voltages is provided during simulations.

BİLEZİKLİ ASENKRON MAKİNE İLE ŞEBEKE BAĞLANTILI DEĞİŞKEN HIZ GENERATÖR UYGULAMASI

Erhan Demirok

EECS, Yüksek Lisans Tezi, 2007

Tez Danışmanı: Prof. Dr. Asıf Şabanoviç

Anahtar Kelimeler: Aktif ve reaktif güç ayrıştırma, generatör, yenilenebilir enerji, bozucu etken gözlemleyici, bilezikli asenkron makina, değişken hızda çalışma

Özet

Genel olarak tezde üzerinde çalışılan konu elektrik şebekesi ile generatör arasındaki güç akışıdır. Elektrik şebekesi ve generatör arasındaki çeşitli bağlantı kavramları tarif edildikten sonra bu kavramlar arasından en verimli olan bilezikli asenkron makine kullanılarak değişken hız sabit frekans topolojisi vurgulanmıştır. Seçilen topolojideki bilezikli asenkron makinenin dinamik modeli çıkarılmış ve güç akış analizine değinilmiştir. Uluslararası yapıtlarda en çok tercih edilen ve uygulama alanı bulan stator akısı yönelimli aktif-reaktif güç ayrışımı yöntemi tezde incelenerek benzetimi yapılmıştır. Yöntemdeki dezavantajlardan kısaca bahsedilerek bu dezavantajların ortadan kaldırılması için bozucu etken gözlemleyicili lineer olmayan denetleyici geliştirildi. Öne sürülen bu yöntemle incelenen güç akışı kavramına referans eksen takımı yöneliminden bağımsızlık ve kolay uygulanabilirlik kazandırıldı. Denetleyici performansı açısından üssel kararlılığı ispatlamak için kararlılık analizi, her tasarımda gerçekleştirilmelidir. Simülasyonlarda, bilezikli asenkron makinesine uygulanan rotor gerilimi nominal değerlerinin altında sınırlı kalmıştır.

“To my family and Diren Feda”

Acknowledgement

I would like to thank my supervisor Asıf ŞABANOVİÇ for help, encouragement and his behaviour to me like a father.

I am grateful to my thesis committee members Ahmet ONAT, Deniz YILDIRIM, Kemalettin ERBATUR, Mahmut AKŞİT for their valuable contribute and review on the thesis.

My sincere thanks to all friends in my life and colleagues at the Mechatronics lab, and Mathematics Program from Sabancı University.

Special thanks goes to Merve ACER, Meltem ELİTAŞ, Erol ÖZGÜR, Asenterabi MALİMA, Esen AKSOY, Özcan YAZICI, Emel YEŞİL, and Alp BASSA who are all great friends who have shared everything they know.

Special acknowledgement must also go to my family for their continuously support and trust throughout the year.

Finally, I am particularly grateful to Diren Feda GÜMÜŞBOĞA for helping and assisting me in all the stages of this work. Her constant and continous co-operation proves her dearness and support during my life.

TABLE OF CONTENTS

LIST OF FIGURES

LIST OF TABLES

TABLE OF SYMBOLS

DFIM	Doubly-fed induction machine
DFIG	Doubly-fed induction generator
PMSM	Permanent Magnet Synchronous Machine
CSCF	Constant speed constant frequency
SCIG	Squirrel cage induction generator
VSCF	Variable speed constant frequency
GSC	Grid side converter
MSC	Machine side converter
PWM	Pulse Width Modulation
U_s	Magnitude of grid voltage
FF	Feedforward
VSC	Voltage source converter
VSS	Variable Structure System

1 INTRODUCTION

Energy production capacity determines the politics decisions-strategies, economical and social developments that make the energy sector to be one of the most critical topic around the world. Alternative resources are becoming more important while fossil based fuels come to an end.

Renewable energy, as its name implies, is an energy source that does not die out and is regenerative. It does not contribute greenhouse materials as fossil fuels do. Renewable energy sources can depend on climate and region conditions. For example, solar hot water/heating is the most widely used application in Turkey with 6.5% of total solar hot water/heating capacity of the world in 2005 [1]. Main renewable energy sources are as follows: Solar cell, wind, hydro power, biofuel (liquid, solid biomass, biogas), geothermal energy [2]. Figure 1.1 shows the world renewable energy pie chart in 2005 [2].

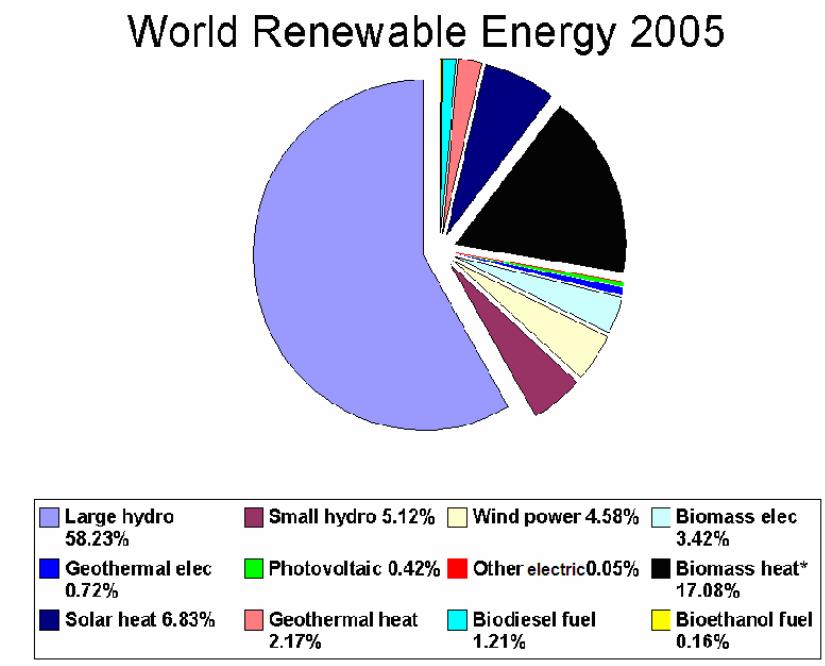

Figure 1.1. World renewable energy pie chart [1]

Although utilizable energy production methods varies with respect to renewable energy sources, the main objective is to develop an universal and autonomous configuration for grid connected or stand-alone applications with realization of some mechanical constraints (shaft angular speed etc.) and independent of energy source type.

1.1 Motivation and System Overview

From the generator point of view, energy source is always prime movers excited by renewable sources through turbines. These sources may change at any time dynamically like wind or water but injected power fluctuations to the grid must be removed for grid connected applications while produced voltage must have constant magnitude and constant frequency for stand alone applications. When considering overall structure, electrical machines play an important role for system efficiency and must be utilized optimally by selecting proper machine type. Accordingly, three different types of electrical machines are usually assigned to renewable energy plants as generator: Permanent magnet synchronous, synchronous, and induction machines.

Permanent magnet synchronous machines (PMSM) have constant field excitation rotating with same rotor mechanical speed because of permanent rare earth magnets (neodymium and samarium-cobalt) located on the rotor and have armature on the stator with isolated windings. Since field excitation is constant and not controllable, stator current can be controlled via an inverter attached on stator.

Synhronous machines are similar to PMSMs except for rotor construction. Stator has three-phase windings. In contrast to PMSMs, the rotor of synchronous machines has winding on the rotor and a dc current is supplied to create a field. Generator operation is determined by the magnitude of the dc current (field current) and rotor angular speed.

Induction machines are the most widespread in industry. By the improvements in the power electronics, induction machine applications come to a level that high precision torque/position control devices are available to run IM motor with while having realtively low costs in comparison with other drives. Stationary part of an induction machine is similar to the one that is described for PMSM and synchronous

machine. Induction machines can be divided two main structures up to their rotor construction: squirrel cage and wound rotor (doubly-fed). The rotor of squirrel cage machines consists of conductive bars with their slots and end points of similar phase bars are short circuited. The rotor windings of wound rotor machines have the same structure with stator windings and ac rotor voltages are applied via ring and brush mechanism. The rotor current magnitude and frequency are controlled in such a way that stator voltage with fixed magnitude and frequency is generated while angular speed of rotor varies.

Induction generators have some advantages over permanent magnet and synchronous generators for renewable energy systems. Induction machines are cheaper than permanent magnet synchronous machines, since permanent magnets are expensive, especially for high power rated generators. Furthermore, synchronous generators must operate at constant rotor speed for fixed frequency so it will require more complicated mechanics between energy source and generator shaft.

Renewable energy system concepts (e.g. wind, small hydro plant) can be classified with respect to the generator shaft speed (prime mover speed) and electrical output frequency: Constant speed constant frequency, variable speed constant frequency.

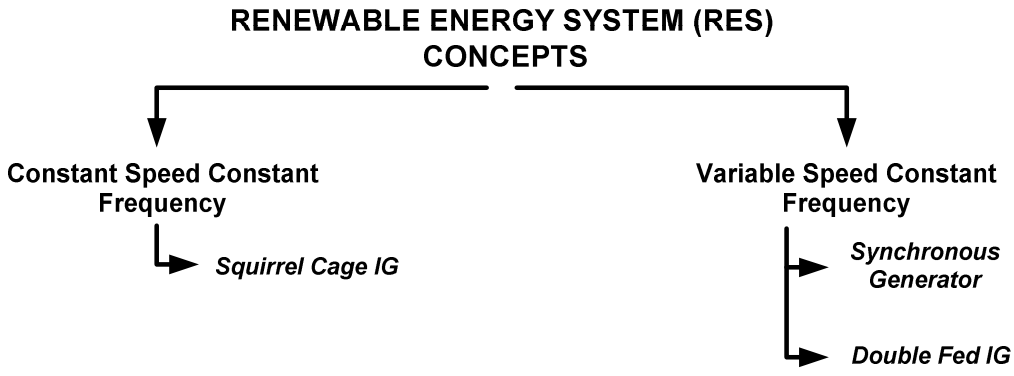

Figure 1.2. Summary of renewable energy system concepts

Constant-speed constant-frequency (CSCF) squirrel cage induction generator (SCIG) concept transforms renewable energy source into electrical energy in such a way that SCIG is directly connected to grid (Figure 1.3). Since cost is lower and electronic-

mechanic complexity is reduced, CSCF concept has been the most used configuration in wind turbine applications [3]. Fixed turbine speed is implemented by gear box with turbine stall-pitch control and poles of the generator. In this way, squirrel cage induction generators with at least two different pole stages are usually used. Different pole-number stages will decrease magnetizing losses at low turbine speed [4].

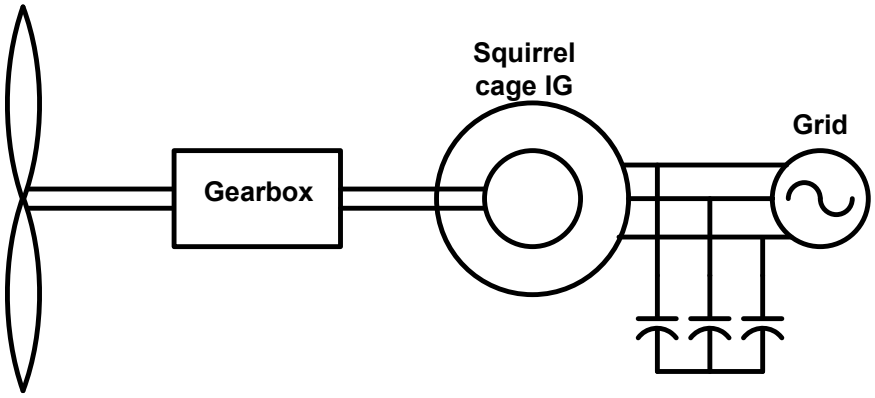

Figure 1.3. Constant-speed constant-frequency concept with SCIG

SCIGs require reactive power for both motor and generator operations. The most of reactive power drawn by SCIG is supplied by compansator capacitors which is the most economical way for SCIG power factor control at its stator terminal (Figure 1.3). This concept is valid for grid-connected applications.

Variable speed constant frequency (VSCF) concept is usually accomplished by using either synchronous generator (alternatively SCIGs are used) or doubly fed induction generator (DFIG). Fixed speed turbine is not required but still voltage frequency and amplitude must be fixed for stand-alone or grid-connected applications. Energy capture is more efficient than fixed speed concept because of variable speed operation.

VSCF concept using synchronous generator requires back-to-back pwm converter for grid integration (Figure 1.4). Since turbine speed is varying, stator frequency and voltage magnitude must be kept constant by back-to-back pwm converter connected between stator of the generator and the grid. The pwm converter must handle the active and reactive power produced by the generator including the overload conditions. While grid side converter (GSC) provides unity power factor and regulation of dc bus voltage,

machine side converter (MSC) controls the active power. In this scheme, instead of synchronus generator, SCIG and PMSM may be utilized.

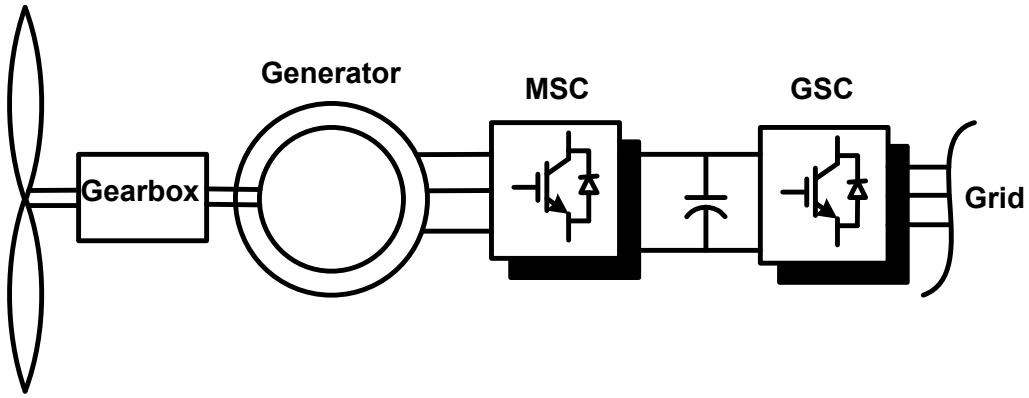

Figure 1.4. Variable-speed constant-frequency concept (direct in-grid)

Besides on VSCF with direct in-grid concept, another concept is VSCF with doubly-fed induction generator (DFIG). Although they are rarely used in industry, doubly-fed induction machines can find applications in which high starting torque in the motor mode is required like cranes, extruders etc. The easiest way to accomplish these applications is to add or remove external resistors to rotor circuits through ring and brushes for adjustment of rotor current. Although torque-speed characteristics can be shifted to desired operation point using external resistors, the method is inefficient on account of power dissipation on resistors. Alternative method is to feed this dissipated power back to the grid exactly same with Scherbius systems. Accordingly, back-to-back pwm converter attached to the rotor of DFIG will bring to the system an advantage that active and reactive power can be decoupled and also bidirectional power flow for sub- or supersynchronous operation while the converter is considered as variable resistor (Figure 1.5).

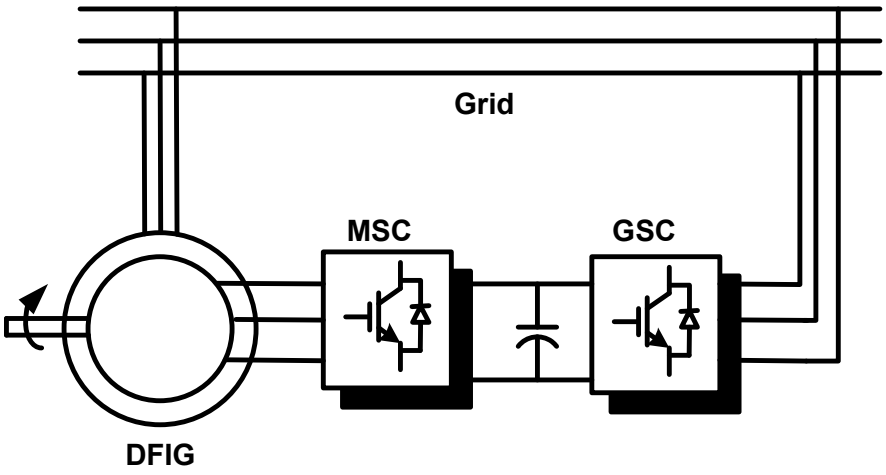

Figure 1.5. Variable-speed constant-frequency concept with DFIG

The back-to-back pwm converter's operation is the same for the VFCG one but the power rating of converter will be about 25% of the system power because the converter is attached to the rotor side. The rotor of DFIG will draw power during sub-synchronous operation (rotor mechanical speed is lower than synchronous speed) while the rotor and stator will supply grid during super-synchronous operation. Hence, the back-to-back pwm converter is also convenient in bidirectional power flow point of view.

The reasons for using doubly fed induction machine are as follows:

- Reduced cost and size
- Absence of separate direct current (dc) supply
- Stator active and reactive power control (power factor) is accomplished via rotor currents so rated converter size will be around 25% of the overall system power [5]
- The back-to-back pwm converter will have less losses so system efficiency increases.

In this thesis, the operation of the doubly-fed (wound rotor) induction machine (DFIM) as generator for variable speed renewable energy systems like wind or small hydro plant applications will be analysed. The goal is to develope and build a system in such a way that generated active and reactive power can be controlled as rotor

mechanical speed varies for both grid-connected and stand-alone operations. The outline is depicted in Figure 1.6.

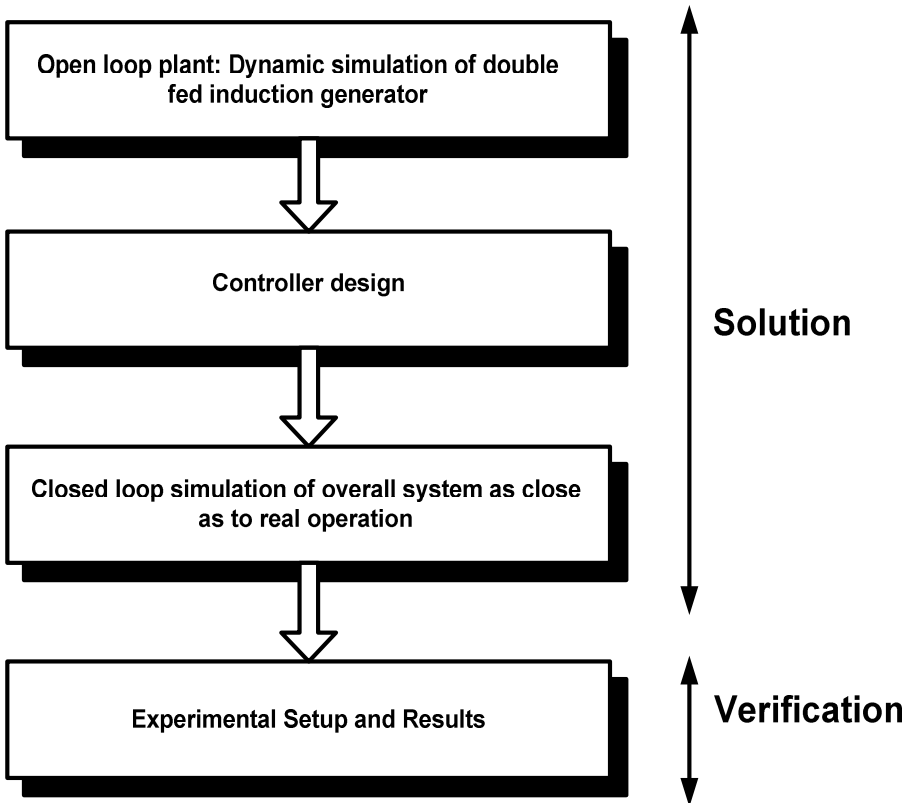

Figure 1.5. General outline

.

2 AC MACHINE THEORY AND DYNAMICAL ANALYSIS OF DOUBLY FED INDUCTION MACHINE

Since the equivalent circuit model is insufficient in transient state, a dynamical model which includes transient and steady state conditions must be developed for applications where states and parameters are varying. In this chapter, firstly, a general AC machinery fundamentals will be introduced by emphasizing magnetic circuit theory using phasor representations with some assumptions. After electrical and mechanical equations are derived, a dynamical model of doubly fed induction machine is completed. Simulation results are interpreted by space vector analysis.

2.1 Review of Basic Concepts of Magnetic Circuit Theory

From engineering point of view, a problem should be well-defined as first step while mathematical derivation is the second step for developing model. Similarly, magnetic circuit theory gives an opportunity to understand ac machines physically and gives mathematical tools to analyse the system behaviour.

Three basic concepts are sufficient to understand ac machinery fundamentals:

- Ampere's Law
- Faraday's Law

Electromagnetic force to convert electrical energy into mechanical motion.

2.1.1 Ampere's Law

A magnetic field is produced when a current source exists and current flows through a conductor. The direction and magnitude of magnetic field depend on the direction and magnitude of current respectively. Ampere's law explains this situation as following: The line integral of flux density around any closed path that encloses a current flowing conductor is equal to permeability times this current (Figure 2.1).

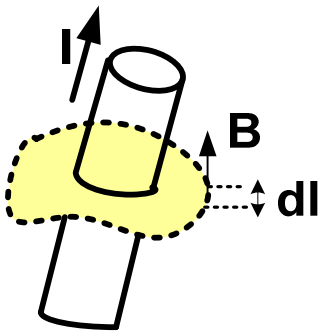

Figure 2.1. Ampere's Law representation

$$\oint Bdl = \mu_m I \quad \text{or} \quad \oint Hdl = I \tag{2.1}$$

where B is flux density, H is magnetic field intensity, μ_m is permeability of material that magnetic field passes, and I is total current enclosed by closed path.

The relationship between field intensity and flux density for any ferromagnetic material is not linear for all operating range although $B = \mu_m H$ is valid. There exists a limiting value of field intensity for which saturation effect occurs because of nonlinear B-H characteristics of ferromagnetic materials. Linear region constraint should be considered or an assumption must be held in such a way that saturation effect does not exist.

Flux and flux linkage are obtained by using definition of flux density. Accordingly, flux is calculated with limited area A_m perpendicular to the direction of flux density.

$$\phi = A_m B$$

When flux is linked by some number of turns (N) of a coil, flux linkage is defined as

$$\lambda = N\phi$$

2.1.2 Faraday's Law

According to Faraday's law, the induced electromotive force (emf) is proportional to the time rate of change of flux through the circuit or coil. Flux varying with time can be obtained by changing magnetic field strength, moving coil or magnet relative to each other.

$$e(t) = \frac{d}{dt}\lambda(t) = \frac{d}{dt}(N\phi(t)) \tag{2.2}$$

where emf (e(t)) denotes the induced or generated voltage.

2.1.3 Electromagnetic Force

When a uniform magnetic field that is perpendicular to length of conductor is applied to a current flowing conductor, a electromagnetic force is resulted on the conductor (Figure 2.2).

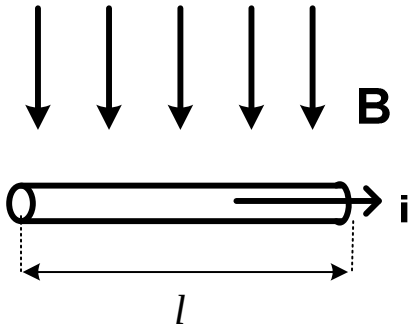

Figure 2.2. Electromagnetic force on a current flowing conductor

$$f_{em} = i * \vec{l} \times \vec{B} \tag{2.3}$$

where units are as follows: *B* is [T], *i* is [A], and ℓ is [m].

2.2 Generalized AC Machine Model

For the simplification of mathematical model of ac machine, some assumptions must be presented:

- Saturation and slot effects of stator and rotor iron core are neglected
- Permeability of stator and rotor iron core is infinite
- Airgap flux distribution is sinusoidal (the number of turns of windings are distributed sinusoidally for low harmonic content)
- Stator and rotor windings are star-connected and neutrals of the windings are isolated for stator and rotor in case of doubly fed induction machine.
- Supplied voltages/currents are symmetrical

$$i_{s1}(t) + i_{s2}(t) + i_{s3}(t) = 0$$

Figure 2.3 shows the cutaway diagram of a generalized ac machine. α is stator angle that scans all stator windings at any time with respect to axis of stator winding *U* as reference. In case of stator winding *V*, reference frame will be located with 120° and 240° for winding *W*. β is rotor angle with respect to axis of rotor winding *U*. θ is the angle between rotor and stator windings *U*. It also determines mechanical angle and rotor mechanical speed.

$$\omega = \frac{d\theta}{dt} \tag{2.4}$$

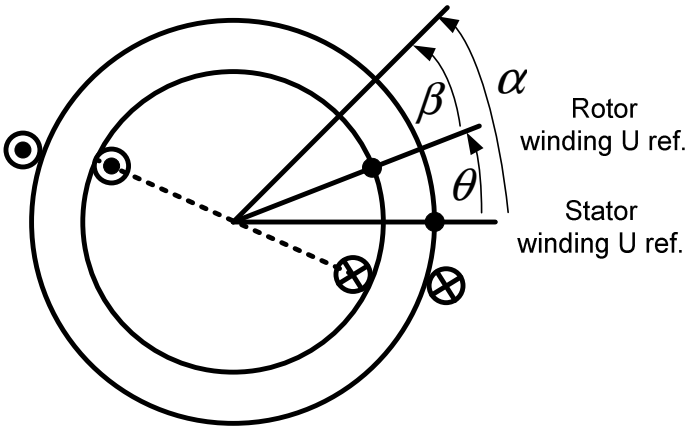

Figure 2.3. Cut-away view of ac machine

To compute stator and rotor flux linkages, ampereturns should be calculated first. Because both stator and rotor windings are distributed sinusoidally, a sinusoidal function term or conductor density term must be multiplied by the number of turns *N* directly

$$q(\alpha) = \cos\alpha \tag{2.5}$$

or winding distribution in terms of α at time *t*

$$n_s(\alpha,t) = \hat{n}_s \cos\alpha$$

$$N_s = \int_{-\frac{\pi}{2}}^{\frac{\pi}{2}} n_s(\alpha,t)d\alpha = \int_{-\frac{\pi}{2}}^{\frac{\pi}{2}} \hat{n}_s \cos\alpha d\alpha = 2\hat{n}_s$$

$$n_s(\alpha,t) = \frac{N_s}{2}\cos\alpha \tag{2.6}$$

Therefore, ampereturn (mmf) can be written for all three phase stator windings as follows:

$$mmf_s(\alpha,t) = (N_s i_{s1}(t)\cos\alpha) + (N_s i_{s2}(t)\cos(\alpha - \frac{2\pi}{3})) + (N_s i_{s3}(t)\cos(\alpha - \frac{4\pi}{3}))$$

$$mmf_s(\alpha,t) = N_s\left[i_{s1}(t)\cos\alpha + i_{s2}(t)\cos(\alpha - \frac{2\pi}{3}) + i_{s3}(t)\cos(\alpha - \frac{4\pi}{3}) \right] \qquad (2.7)$$

where N_s is the number of turns for each stator phase. For the sake of simplicity, if equation (2.7) is transformed to complex plane

$$\cos\alpha = \frac{e^{j\alpha} + e^{-j\alpha}}{2}$$

$$mmf_s(\alpha,t) = N_s\left[i_{s1}(t)\frac{e^{j\alpha} + e^{-j\alpha}}{2} + i_{s2}(t)\frac{e^{j(\alpha-\frac{2\pi}{3})} + e^{-j(\alpha-\frac{2\pi}{3})}}{2} + i_{s3}(t)\frac{e^{j(\alpha-\frac{4\pi}{3})} + e^{-j(\alpha-\frac{4\pi}{3})}}{2} \right]$$

$$mmf_s(\alpha,t) = \frac{N_s}{2}\left[e^{j\alpha}\left(i_{s1}(t) + i_{s2}(t)e^{-j\frac{2\pi}{3}} + i_{s3}(t)e^{-j\frac{4\pi}{3}} \right) + e^{-j\alpha}\left(i_{s1}(t) + i_{s2}(t)e^{j\frac{2\pi}{3}} + i_{s3}(t)e^{j\frac{4\pi}{3}} \right) \right]$$

$$mmf_s(\alpha,t) = \frac{N_s}{2}\left[e^{-j\alpha}\bar{i}_s(t) + e^{j\alpha}\bar{i}^*_s(t) \right] \qquad (2.8)$$

or

$$mmf_s(\alpha,t) = \frac{N_s}{2}\mathrm{Re}\left\{ e^{-j\alpha}\bar{i}_s(t) + e^{j\alpha}\bar{i}_s{}^*(t) \right\} \qquad (2.9)$$

where $\bar{i}_s(t)$ represents stator current vector in complex plane (see 2.9).

$$\bar{i}_s(t) = i_{s1}(t) + i_{s2}(t)e^{j\frac{2\pi}{3}} + i_{s3}(t)e^{j\frac{4\pi}{3}} = i_s(t)e^{j\zeta(t)} \qquad (2.10)$$

Combining (2.10) into (2.9), ampereturn becomes

$$mmf_s(\alpha,t) = \frac{N_s}{2}\left[i_s(t)e^{j(\zeta-\alpha)} + i_s(t)e^{-j(\zeta-\alpha)} \right] = N_s i_s(t)\left[\frac{e^{j(\zeta-\alpha)} + e^{-j(\zeta-\alpha)}}{2} \right]$$

$$mmf_s(\alpha,t) = N_s i_s(t)\cos\left(\zeta(t) - \alpha\right) \qquad (2.11)$$

As seen from equation (2.11), stator ampereturn vector has a sinuisoidal pulsation for any given α and it can be represented by a rotating vector with constant amplitude and speed in the air gap.

The same derivations are also valid for rotor ampereturns.

$$mmf_r(\beta,t) = N_r\left[i_{r1}(t)\cos\beta + i_{r2}(t)\cos\left(\beta - \frac{2\pi}{3}\right) + i_{r3}(t)\cos\left(\beta - \frac{4\pi}{3}\right)\right]$$

$$mmf_r(\beta,t) = \frac{N_r}{2}\left[e^{-j\beta}\bar{i}_r(t) + e^{j\beta}\bar{i}_r^{\,*}(t)\right]$$

since $\beta = \alpha - \theta$ (Figure 2.3)

$$mmf_r(\alpha,\theta,t) = \frac{N_r}{2}\left[e^{-j(\alpha-\theta)}\bar{i}_r(t) + e^{j(\alpha-\theta)}\bar{i}^{\,*}_r(t)\right] \qquad (2.12)$$

$$mmf_r(\alpha,\theta,t) = N_r i_r(t)\cos(\alpha - \theta - \xi(t)) \qquad (2.13)$$

Total ampereturns can be calculated directly as

$$mmf(\alpha,\theta,t) = mmf_s(\alpha,t) + mmf_r(\alpha,\theta,t)$$

The permeability of iron core is assumed to be infinite, and flux density is derived at both sides of airgap by reducing rotor flux density to stator and stator flux density to rotor. Flux density that appears on the stator side of airgap,

$$B_s(\alpha,\theta,t) * L = \mu_0\left(mmf_s(\alpha,t) + K * mmf_r(\alpha,\theta,t)\right)$$

where *K* is leakage flux constant which takes values between 0 and 1, *L* is radially length between stator and rotor (airgap). Using the symmetric and sinusoiadally distributed properties of stator windings,

$$B_s(\pi + \alpha + \zeta) = -B_s(\alpha + \zeta)$$

and if the sign of magnetic field density is considered as positive when the field direction is away from center of rotor,

$$B_s(\alpha+\zeta)*l_{gap}-(-B_s(\pi+\alpha+\zeta))*l_{gap}=\mu_0*(mmf_s(\alpha,t)+K*mmf_r(\alpha,\theta,t))$$

$$B_s(\alpha,\theta,t)=\frac{1}{2l_{gap}}\mu_0[mmf_s(\alpha,t)+K*mmf_r(\alpha,\theta,t)] \qquad (2.14)$$

Flux can be obtained from flux density by calculation of cross-section area in that flux density passes through.

$$\phi_s(\alpha,\theta,t)=B_s(\alpha,\theta,t)A_{core}$$

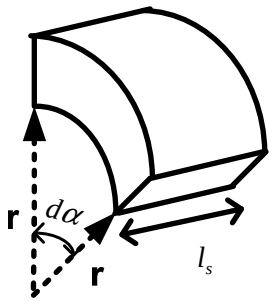

Figure 2.4. Cross-section area of flux

As seen from Figure 2.4, cross-section area becomes

$$A_{core}=r*(d\alpha)*l_s$$

$$\phi_s(\alpha,\theta,t)=\int_{\alpha=\varepsilon-\frac{\pi}{2}}^{\varepsilon+\frac{\pi}{2}}B_s(\alpha,\theta,t)*r*l_s*d\alpha \qquad (2.15)$$

Since the windings are distrubuted sinusoiadally, flux linkage is derived by integration of equations (2.6) times (2.15) between $-\frac{\pi}{2}$ and $\frac{\pi}{2}$.

$$\lambda_{s1}(t) = \int_{\varepsilon=-\frac{\pi}{2}}^{\frac{\pi}{2}} \int_{\alpha=\varepsilon-\frac{\pi}{2}}^{\varepsilon+\frac{\pi}{2}} \left[\left(\frac{N_s}{2} \cos\varepsilon \right) B_s(\alpha,\theta,t) r * l * d\alpha * d\varepsilon \right] \tag{2.16}$$

Flux linkage derivations for stator winding 2 and 3 are the same with stator winding 1 but only integral boundary ranges are different in such a way that their corresponding reference frames are shifted away $\frac{2\pi}{3}$ and $\frac{4\pi}{3}$ respectively.

Using equations (2.8), (2.12), (2.14), and (2.16), the result of integration becomes

$$\lambda_{s1}(t) = \frac{L_s}{3}\left[\bar{i}_s(t) + \bar{i}^{\circ}{}_s(t)\right] + \frac{L_m}{3}\left[\bar{i}_r(t)e^{j\theta} + \bar{i}^{*}{}_r(t)e^{-j\theta}\right] \tag{2.17}$$

where $L_s = \frac{3}{8}\frac{N_s{}^2 l_s r\pi\mu_0}{l_{gap}}$ and $L_m = \frac{3}{8}\frac{KN_s N_r l_r r\pi\mu_0}{l_{gap}}$, $l_s = l_r$

$$\lambda_{s2}(t) = \frac{L_s}{3}\left[\bar{i}_s(t)e^{-j\frac{2\pi}{3}} + \bar{i}^{*}{}_s(t)e^{j\frac{2\pi}{3}}\right] + \frac{L_m}{3}\left[\bar{i}_r(t)e^{j(\theta-\frac{2\pi}{3})} + \bar{i}^{*}{}_r(t)e^{-j(\theta-\frac{2\pi}{3})}\right] \tag{2.18}$$

$$\lambda_{s3}(t) = \frac{L_s}{3}\left[\bar{i}_s(t)e^{-j\frac{4\pi}{3}} + \bar{i}^{*}{}_s(t)e^{j\frac{4\pi}{3}}\right] + \frac{L_m}{3}\left[\bar{i}_r(t)e^{j\left(\theta-\frac{4\pi}{3}\right)} + \bar{i}^{*}{}_r(t)e^{-j\left(\theta-\frac{4\pi}{3}\right)}\right] \tag{2.19}$$

Finally, stator flux linkage can be represented in complex vector as

$$\bar{\lambda}_s(t) = L_s\bar{i}_s(t) + L_m\bar{i}_r(t)e^{j\theta(t)} \tag{2.20}$$

where $\bar{\lambda}_s(t) = \lambda_{s1}(t) + \lambda_{s2}(t)e^{j\frac{2\pi}{3}} + \lambda_{s3}(t)e^{j\frac{4\pi}{3}}$

As seen from equation (2.20), rotor current effects on stator flux linkage with rotor mechanical angle.

Rotor flux linkage is calculated in the same manner with stator flux linkage. Accordingly,

$$\lambda_{r1}(t) = \frac{L_r}{3}\left[\bar{i}_r(t) + \bar{i}^*_r(t)\right] + \frac{L_m}{3}\left[\bar{i}_s(t)e^{-j\theta} + \bar{i}^*_s(t)e^{j\theta}\right] \tag{2.21}$$

$$\lambda_{r2}(t) = \frac{L_r}{3}\left[\bar{i}_r(t)e^{-j\frac{2\pi}{3}} + \bar{i}^*_r(t)e^{j\frac{2\pi}{3}}\right] + \frac{L_m}{3}\left[\bar{i}_s(t)e^{-j(\theta+\frac{2\pi}{3})} + \bar{i}^*_s(t)e^{j(\theta+\frac{2\pi}{3})}\right] \tag{2.22}$$

$$\lambda_{r3}(t) = \frac{L_r}{3}\left[\bar{i}_r(t)e^{-j\frac{4\pi}{3}} + \bar{i}^*_r(t)e^{j\frac{4\pi}{3}}\right] + \frac{L_m}{3}\left[\bar{i}_s(t)e^{-j(\theta+\frac{4\pi}{3})} + \bar{i}^*_s(t)e^{j(\theta+\frac{4\pi}{3})}\right] \tag{2.23}$$

where $L_r = \frac{3}{8}\frac{N_r{}^2 l_r r\pi\mu_0}{l_{gap}}$ is the self inductance of rotor. Rotor flux linkage can be represented in complex vector combining (2.21)-(2.23)

$$\bar{\lambda}_r(t) = L_r\bar{i}_r(t) + L_m\bar{i}_s(t)e^{-j\theta} \tag{2.24}$$

According to Faraday's Law, the rate of change of flux linkage will induce a voltage. Therefore, stator and rotor equivalent circuits can be shown roughly in terms of flux linkages in Figure 2.5.

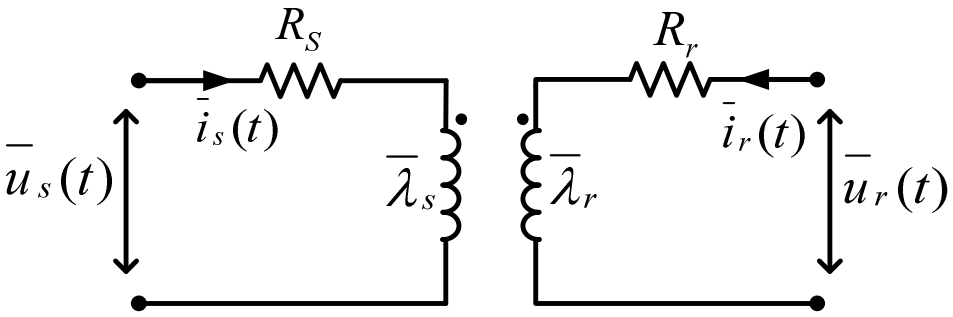

Figure 2.5. Stator and rotor equivalent circuit

The induced (emf) stator voltage for one phase is computed as

$$u_{s1}(t) = R_s i_{s1}(t) + \frac{d}{dt}\left(\lambda_{s1}(t)\right) \tag{2.25}$$

The other stator voltages $u_{s2}(t)$ and $u_{s3}(t)$ are determined in the same manner with equation (2.25) using their corresponding stator currents and flux linkages. In complex vector, stator voltage in stator reference frame becomes

$$\bar{u}_s(t) = R_s \bar{i}_s(t) + \frac{d}{dt}\left(\bar{\lambda}_s(t)\right) = R_s \bar{i}_s(t) + \frac{d}{dt}\left(L_s \bar{i}_s(t) + L_m \bar{i}_r(t) e^{j\theta(t)}\right)$$

$$\bar{u}_s(t) = R_s \bar{i}_s(t) + L_s \frac{d\bar{i}_s(t)}{dt} + L_m \left[\frac{d\bar{i}_r(t)}{dt} e^{j\theta(t)} + \bar{i}_r(t) \frac{d}{dt}\left(e^{j\theta(t)}\right)\right]$$

$$\bar{u}_s(t) = R_s \bar{i}_s(t) + L_s \frac{d\bar{i}_s(t)}{dt} + L_m \frac{d\bar{i}_r(t)}{dt} e^{j\theta(t)} + j\omega L_m \bar{i}_r(t) e^{j\theta(t)} \tag{2.26}$$

As seen from last two terms of equation (2.26), stator voltage depends on mutual inductance and rotor mechanical speed with combination of rotor current.

Rotor voltage equations are also derived in the same way according to rotor reference frame as follows

$$\bar{u}_r(t) = R_r \bar{i}_r(t) + \frac{d}{dt}\left(\bar{\lambda}_r(t)\right) \tag{2.27}$$

Using equations (2.24) and (2.27)

$$\bar{u}_r(t) = R_r \bar{i}_r(t) + L_r \frac{d\bar{i}_r(t)}{dt} + L_m \frac{d\bar{i}_s(t)}{dt} e^{-j\theta(t)} - j\omega L_m \bar{i}_s(t) e^{-j\theta(t)} \tag{2.28}$$

Since the rotor windings are short circuited at the end points for squirrel cage induction machine, the rotor voltage becomes zero ($\bar{u}_r(t) = 0$). In the case of doubly-fed induction motor, $\bar{u}_r(t)$ will be injected from an external source via brush-ring mechanism.

Mechanical/electromechanical equations are required to complete the machine model besides on electrical equations. Since generated flux density on the rotor side of airgap will act as a tangential electromagnetic force on the sinusoidally distributed rotor windings, torque will be achieved. The flux density that appears on the rotor side of airgap,

$$B_r(\beta,\alpha,t) = \frac{1}{2l_{gap}}\mu_0\left[mmf_r(\beta,t) + K * mmf_s(\alpha,t)\right] \tag{2.29}$$

since equation (2.29) is written in the rotor reference frame, $mmf_s(\alpha,t)$ must be first converted to the rotor reference frame by using $\alpha = \beta + \theta$ and equation (2.8) (Figure 2.3)

$$mmf_s(\beta,\theta,t) = \frac{N_s}{2}\left[\bar{i}_s(t)e^{-j(\beta+\theta)} + \bar{i}^*_s(t)e^{j(\beta+\theta)}\right] \tag{2.30}$$

An important point that makes the flux density on the rotor simplified is elimination of the first term $mmf_r(\beta,t)$ in (2.29) beacuse of uniform airgap. The rotor currents will not effect on the flux density that appears on the rotor. This situation can be observed by using equation (2.29) for torque computation [6]. Consequently, (2.29) is modified as

$$B_r(\beta,\theta,t) = \frac{1}{2l_{gap}}\mu_0 K mmf_s(\beta,\theta,t) \tag{2.31}$$

Combining (2.30) and (2.31),

$$B_r(\beta,\theta,t) = \frac{\mu_0 K N_s}{4l_{gap}}\left[\bar{i}_s(t)e^{-j(\beta+\theta)} + \bar{i}^*_s(t)e^{j(\beta+\theta)}\right] \tag{2.32}$$

and electromagnetic force is depicted in Figure 2.6.

As mentioned earlier (2.3), electromagnetic force depends on the rotor current, length of rotor axis, and the flux density that is computed yet in (2.32). Since rotor

windings are sinusoidally distributed, rotor current distribution must be defined first to derive electromagnetic force and mechanical torque.

$$df_{em} = -B_r(\beta,\theta,t) * \sigma(\beta,t) * l * r * d\beta \tag{2.33}$$

where $\sigma(\beta,t)$ is current distribution, $rd\beta$ is unit arc length along rotor surface.

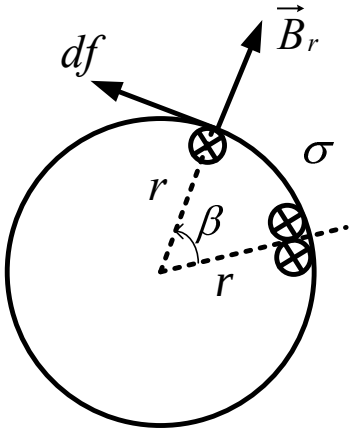

Figure 2.6. Electromagnetic force acting on the rotor windings

Rotor current distribution can be defined intuitively as the derivative of $mmf_r(\beta,t)$ with respect to unit arc length along rotor surface [6].

$$\sigma(\beta,t) = \frac{1}{2}\frac{\partial}{\partial(r\beta)} mmf_r(\beta,t) \tag{2.34}$$

Using equations (2.33) and (2.34), torque is calculated for integral boundary $0 \le \beta \le 2\pi$ as

$$\tau_{em}(t) = \oint r * df_{em}$$

$$\tau_{em}(t) = \frac{L_m}{3}\left[\bar{i}_s(t)\bar{i}^*_r(t)e^{-j\theta} - \bar{i}^*_s(t)\bar{i}_r(t)e^{j\theta}\right] = \frac{L_m}{3}\left[\bar{i}_s(t)\left(\bar{i}_r(t)e^{j\theta}\right)^* - \bar{i}^*_s(t)\left(\bar{i}_r(t)e^{j\theta}\right)\right] \tag{2.35}$$

if current complex vectors are defined

$$\begin{aligned} \bar{i}_s &= i_{sx} + j i_{sy} \\ \bar{i}_r &= i_{rx} + j i_{ry} \end{aligned} \tag{2.36}$$

then electromagnetic torque can be derived as

$$\tau_{em}(t) = j\frac{2}{3}L_m\left(i_{sy}i_{rx} - i_{sx}i_{ry}\right) \tag{2.37}$$

or

$$\tau_{em}(t) = \frac{2}{3}L_m \operatorname{Im}\left\{\bar{i}_s(t)\left(\bar{i}_r(t)e^{j\theta(t)}\right)^*\right\} \tag{2.38}$$

Equation (2.38) can also be shown in terms of vector product in such a way that

$$\bar{i}_s(t)\left(\bar{i}_r(t)e^{j\theta(t)}\right)^* = \bar{i}_s(t)\times\left(\bar{i}_r(t)e^{j\theta(t)}\right) \tag{2.39}$$

Accordingly, it can be concluded that electromagnetic torque is proportional to the vector product of stator and rotor currents.

$$\tau_{em}(t) \propto \left[\bar{i}_s(t)\times\left(\bar{i}_r(t)e^{j\theta(t)}\right)\right]$$

All derived electrical and mechanical equations that determine transient and steady state model are summarized as follows,

$$\begin{aligned} \bar{u}_s(t) &= R_s\bar{i}_s(t) + L_s\frac{d\bar{i}_s(t)}{dt} + L_m\frac{d\bar{i}_r(t)}{dt}e^{j\theta(t)} + j\omega L_m\bar{i}_r(t)e^{j\theta(t)} \\ \bar{u}_r(t) &= R_r\bar{i}_r(t) + L_r\frac{d\bar{i}_r(t)}{dt} + L_m\frac{d\bar{i}_s(t)}{dt}e^{-j\theta(t)} - j\omega L_m\bar{i}_s(t)e^{-j\theta(t)} \\ J\frac{d\omega}{dt} + \tau_{load}(t) &= \frac{2}{3}L_m\operatorname{Im}\left\{\bar{i}_s(t)\left(\bar{i}_r(t)e^{j\theta(t)}\right)^*\right\} \\ \omega &= \frac{d\theta}{dt} \end{aligned} \tag{2.40}$$

where J is equivalent inertia reduced to ac machine shaft $J = J_m + n^2 J$.

Since above rotor and stator equations are derived according to their own reference frames, they can be written in a common frame. Next chapter will deal with

advantages of stator flux frame so doubly fed induction machine equations that will be used for model should be written in stator flux reference frame. Reference frames transformation angles are depicted in Figure 2.7.

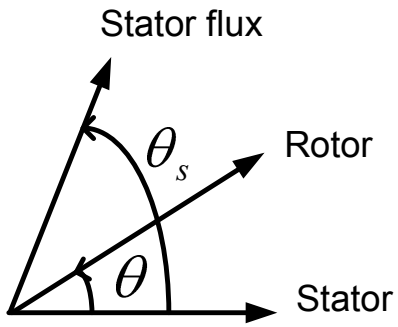

Figure 2.7. Reference frames transformation angles

Superscripts (s), (r), and (e) indicate stator, rotor, and stator flux linkage reference frames respectively. A simple transformation for stator flux linkage is as follows

$$\bar{\lambda}_s^{(s)} = \bar{\lambda}_s^{(e)} e^{j\theta}$$

$$\bar{i}_r^{(r)} = \bar{i}_r^{(e)} e^{j(\theta_s - \theta_r)}$$

If stator and rotor flux linkages are written in stator flux reference frames using equations (2.20) and (2.24)

$$\bar{\lambda}_s^{(e)} e^{j\theta_s} = L_s \bar{i}_s^{(e)} e^{j\theta_s} + L_m \bar{i}_r^{(e)} e^{j(\theta_s - \theta_r)} e^{j\theta} \quad \rightarrow \quad \bar{\lambda}_s^{(e)} = L_s \bar{i}_s^{(e)} + L_m \bar{i}_r^{(e)} \quad (2.41)$$

$$\bar{\lambda}_r^{(e)} e^{j(\theta_s - \theta)} = L_r \bar{i}_r^{(e)} e^{j(\theta_s - \theta)} + L_m \bar{i}_s^{(e)} e^{j\theta_s} e^{j\theta} \quad \rightarrow \quad \bar{\lambda}_r^{(e)} = L_r \bar{i}_r^{(e)} + L_m \bar{i}_s^{(e)} \quad (2.42)$$

Rotor and stator voltage equations (2.40) can also be written as follows

$$\bar{u}_s^{(e)} e^{j\theta_s} = R_s \bar{i}_s^{(e)} e^{j\theta_s} + L_s \frac{d}{dt}\left(\bar{i}_s^{(e)} e^{j\theta_s}\right) + L_m \frac{d}{dt}(\bar{i}_r^{(e)} e^{j(\theta_s - \theta)}) e^{j\theta} + jwL_m \left(\bar{i}_r^{(e)} e^{j(\theta_s - \theta)}\right) e^{j\theta}$$

$$\bar{u}_s^{(e)} = R_s \bar{i}_s^{(e)} + L_s \frac{d\bar{i}_s^{(e)}}{dt} + jw_s L_s \bar{i}_s^{(e)} + L_m \frac{d\bar{i}_r^{(e)}}{dt} + jw_s L_m \bar{i}_r^{(e)} \qquad (2.43)$$

$$\bar{u}_r^{(e)} e^{j(\theta_s-\theta)} = R_r \bar{i}_r^{(e)} e^{j(\theta_s-\theta)} + L_r \frac{d}{dt}\left(\bar{i}_r^{(e)} e^{j(\theta_s-\theta)}\right) + L_m \frac{d}{dt}\left(\bar{i}_s^{(e)} e^{j\theta_s}\right) e^{-j\theta} - jwL_m \bar{i}_s^{(e)} e^{j(\theta_s-\theta)}$$

$$\bar{u}_r^{(e)} = R_r \bar{i}_r^{(e)} + L_r \frac{d\bar{i}_r^{(e)}}{dt} + j(w_s - w)L_r \bar{i}_r^{(e)} + L_m \frac{d\bar{i}_s^{(e)}}{dt} + j(w_s - w)L_m \bar{i}_s^{(e)} \qquad (2.44)$$

If complex voltage and current terms are decoupled into real and imaginary parts (eq. (2.36)) with respect to stator reference frame, ie. $\bar{u}_s^{(e)} = u_{sx} + ju_{sy}$, $\bar{i}_s^{(e)} = i_{sx} + ji_{sy}$ using (2.41), (2.42), (2.43), and (2.44)

$$\begin{aligned} u_{sx} &= R_s i_{sx} + \frac{d\lambda_{sx}}{dt} - w_s \lambda_{sy} \\ u_{sy} &= R_s i_{sy} + \frac{d\lambda_{sy}}{dt} + w_s \lambda_{sx} \end{aligned} \qquad (2.45)$$

$$\begin{aligned} u_{rx} &= R_r i_{rx} + \frac{d\lambda_{rx}}{dt} - (w_s - w)\lambda_{ry} \\ u_{ry} &= R_r i_{ry} + \frac{d\lambda_{ry}}{dt} + (w_s - w)\lambda_{rx} \end{aligned} \qquad (2.46)$$

Equations (2.45) and (2.46) will be used for doubly fed induction machine model but for the controller point of view, state space representation is required selecting state variables $\lambda_{sx}, \lambda_{sy}, i_{rx}, i_{ry}$ as shown in equation (2.47) [7]

$$\frac{d\bar{x}}{dt} = A\bar{x} + B_s \bar{u}_s + B_r \bar{u}_r \qquad (2.47)$$

Equation (2.47) shows that the second term ($B_s \bar{u}_s$) is considered as disturbance while the third term ($B_r \bar{u}_r$) is control input.

3 FIELD-ORIENTED CONTROL OF GRID-CONNECTED DOUBLY-FED INDUCTION MACHINE

To this end, electrical and mechanical equations of doubly-fed induction machine are derived. Recalling the motivation and proposal, the goal is to control the active and reactive power flow between stator terminal and grid. Since stator is connected to three-phase symmetrical grid with constant magnitude U_s and frequency ω_0, the objective is realized by two conditions:

- Controlling the magnitude of stator current vector $\bar{i}_s$,
- Controlling the phase angle φ_s between stator current vector and stator voltage vector $\bar{u}_s$

3.1 Theory of Field Orientation and Orhogonal Control of Stator Current

The apparent power of which is seen at stator terminals for three-phase grid

$$S = 3\bar{u}_s \bar{i}_s^* \tag{3.1}$$

where $\bar{u}_s$ is constant (constant magnitude and frequency)(see Figure 3.1 for phasor representation).

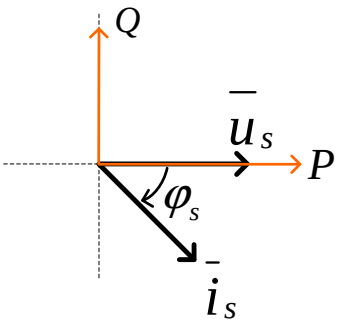

Figure 3.1. Phasor representations of stator current and voltage vectors

Real component of the apparent power is defined as active power P while imaginary part is reactive power Q,

$$S = P + jQ$$

hence active power is projection of stator current vector onto stator voltage vector. P and Q can be written as follows

$$P = 3\left|\bar{u}_s\right|\left|\bar{i}_s\right|\cos\varphi_s \quad \text{and} \quad Q = 3\left|\bar{u}_s\right|\left|\bar{i}_s\right|\sin\varphi_s \tag{3.2}$$

As seen from equations (3.1) and (3.2), active and reactive powers are controlled by stator current magnitude and its phase angle with respect to stator voltage.

After the problem is defined roughly, it is time to find a way that stator current can be controlled via some external control inputs. Doubly-fed induction machine is a strong solution with other advantages mentioned during first chapter for the faced problem. Accordingly, injected rotor currents are usually controlled to supply or draw desired power from stator terminals. The big picture of the overall system is emphasized again in Figure 3.2.

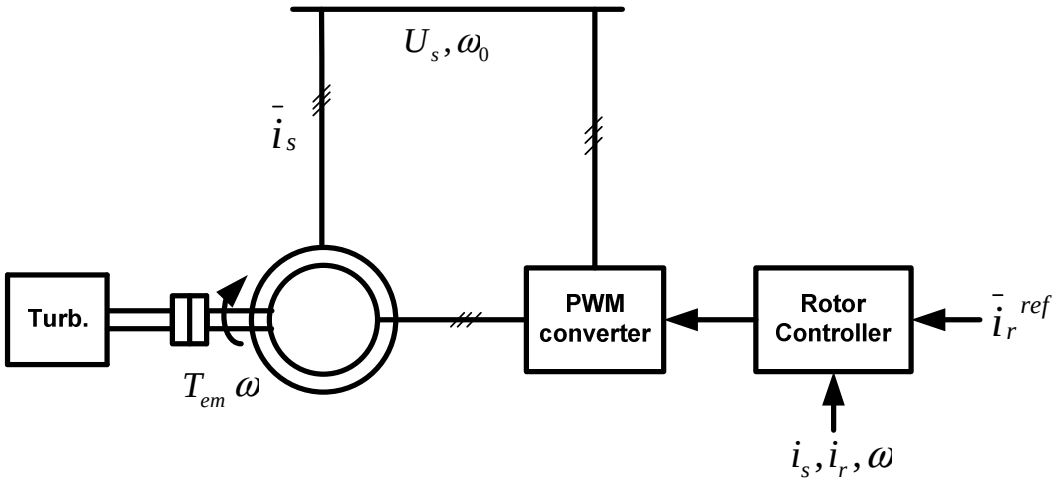

Figure 3.2. Grid-connected doubly-fed induction machine schematic

Before explanation of flux orientation on doubly-fed induction machine, the related assumptions and electrical equations should be given. Assumptions are as follows

- Stator and rotor windings have equal number of turns $N_s = N_r$. Thus, inductances can be easily defined as

$$L_m = L_0 \ , \quad L_s = (1+\sigma_s)L_0, \quad L_r = (1+\sigma_r)L_0 \tag{3.3}$$

  where σ_s and σ_r are leakage factors for stator and rotor rated between (0,1)

- The pwm converter has sufficiently fast current control loop. It means that the pwm converter acts as a current source (Figure 3.2)

- Grid or line has three-phase symmetrical voltage with constant magnitude U_s and frequency ω_0.

$$\bar{u}_s(t) = \frac{3\sqrt{2}}{2} U_s e^{j\omega_0 t} \tag{3.4}$$

where U_s is line-to-neutral rms voltage, and ω_0 is electrical frequency (Figure 3.3).

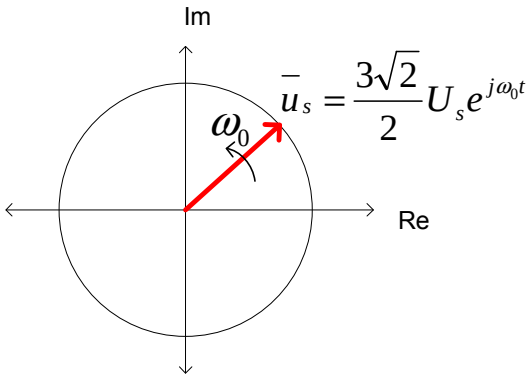

Figure 3.3. Line voltage phasor representation

- Under steady state condition, mechanical speed and load torque is constant

Electrical voltage equations written in their reference frames derived in former chapter are summarized as

$$\begin{aligned} \bar{u}_s(t) &= R_s \bar{i}_s + L_s \frac{d\bar{i}_s}{dt} + L_0 \frac{d}{dt}\left(\bar{i}_r e^{j\varepsilon}\right) \\ \bar{u}_r(t) &= R_r \bar{i}_r + L_r \frac{d\bar{i}_r}{dt} + L_0 \frac{d}{dt}\left(\bar{i}_s e^{-j\varepsilon}\right) \end{aligned} \tag{3.5}$$

For desired active and reactive power, stator current is controlled via rotor current but it requires decoupling of real and imaginary parts of stator current. Thus, active and reactive powers can be controlled independently if stator flux orientation is provided accurately.

Stator flux $\bar{\lambda}_s$ is dependent on magnetizing current $\bar{i}_{ms}$ linearly and using equation (2.20)

$$\bar{\lambda}_s = L_0 \bar{i}_{ms} = (1+\sigma_s) L_0 \bar{i}_s + L_0 \bar{i}_r e^{j\theta}$$

$$\bar{i}_{ms} = (1+\sigma_s)\bar{i}_s + \bar{i}_r e^{j\theta} \tag{3.6}$$

$\bar{i}_{ms}$ or equivalently $\bar{\lambda}_s$ will be chosen as reference frame and it is desired to orient all stator and rotor quantites into this field axis. The reason behind this orientation is explained following sections and reference frames are depicted in Figure 3.4.

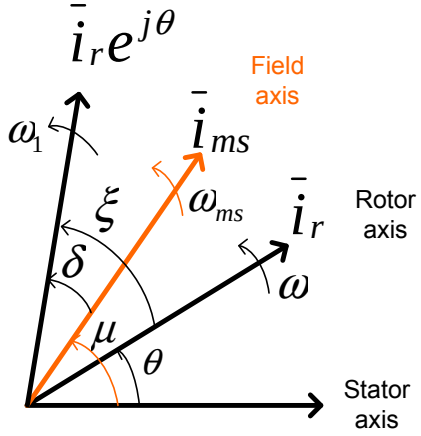

Figure 3.4. Reference frames vector representation

To observe how field orientation provides electromagnetic torque to be controlled by only quadrature component of rotor current and it actually gives an idea about decoupling of stator active power, equation (2.38) is modified.

$$T_{em}(t) = \frac{2}{3} L_0 \operatorname{Im}\left\{\bar{i}_s \left(\bar{i}_r e^{j\theta}\right)^*\right\}$$

The rotor and magnetizing currents in stator coordinates are computed from Figure 3.3

$$\begin{aligned} \bar{i}_r e^{j\theta} &= i_r(t) e^{j(\theta+\xi)} \\ \bar{i}_{ms} &= i_{ms}(t) e^{j\mu} \end{aligned} \tag{3.7}$$

Eliminating stator current in electromagnetic torque using equation (3.6),

$$T_{em} = \frac{2}{3} L_0 \operatorname{Im}\left\{\frac{1}{1+\sigma_s}\left(\bar{i}_{ms} - \bar{i}_r e^{j\theta}\right)\left(\bar{i}_r e^{j\theta}\right)^*\right\}$$

since imaginary part of $\bar{i}_r e^{j\theta}\left(\bar{i}_r e^{j\theta}\right)^*$ is zero,

$$T_{em} = \frac{2}{3}\frac{L_0}{1+\sigma_s}\,\mathrm{Im}\left\{\bar{i}_{ms}\left(\bar{i}_r e^{j\theta}\right)^*\right\}$$

and including equations (3.7)

$$T_{em} = \frac{2}{3}\frac{L_0}{1+\sigma_s}\,\mathrm{Im}\left\{i_{ms}(t)e^{j\mu}\left(i_r(t)e^{j(\theta+\xi)}\right)^*\right\} = -\frac{2}{3}\frac{L_0}{1+\sigma_s} i_{ms}\underbrace{i_r \sin(\theta+\xi-\mu)}_{i_{rq}}$$

$$T_{em} = -\frac{2}{3}\frac{L_0}{1+\sigma_s} i_{ms} i_{rq} \tag{3.8}$$

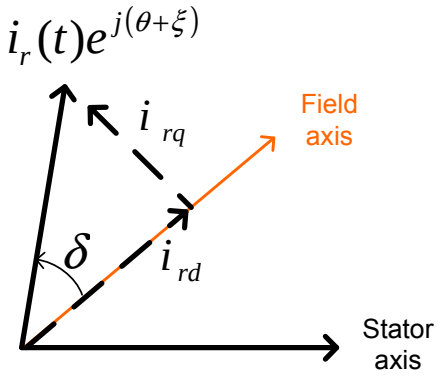

Figure 3.5. Rotor current vector in field coordinates

Equation (3.8) shows that electromagnetic torque can be controlled by quadrature component of rotor current and direct component does not appear in (3.8) (Figure3.5). The same method is performed for decoupling of stator current vector starting from stator voltage and writing it in terms of $\bar{i}_{ms}$ instead of $\bar{i}_s$

$$\bar{u}_s = R_s\bar{i}_s + L_0\frac{d}{dt}\left[(1+\sigma_s)\bar{i}_s + \bar{i}_r e^{j\theta}\right] \tag{3.9}$$

Using (3.6), stator current is eliminated

$$\bar{u}_s = \frac{R_s}{1+\sigma_s}\left(\bar{i}_{ms} - \bar{i}_r e^{j\theta}\right) + L_0\frac{d}{dt}\left[\bar{i}_{ms} - \bar{i}_r e^{j\theta} + \bar{i}_r e^{j\theta}\right]$$

$$\frac{1+\sigma_s}{R_s}\bar{u}_s = \bar{i}_{ms} - \bar{i}_r e^{j\theta} + \underbrace{\frac{(1+\sigma_s)L_0}{R_s}}_{T_s}\frac{d\bar{i}_{ms}}{dt}$$

where $T_s = L_s \big/ R_s$ is defined as stator time constant.

$$T_s \frac{d\bar{i}_{ms}}{dt} + \bar{i}_{ms} = \frac{1+\sigma_s}{R_s}\bar{u}_s + \bar{i}_r e^{j\theta} \tag{3.10}$$

If all terms are written in stator coordinates for common frame, equation (3.10) can be modified. In stator coordinates, the magnetizing current, stator voltage, and rotor current are computed as follows

$$\begin{aligned} \bar{i}_{ms} &= i_{ms}(t)e^{j\mu} \\ \bar{u}_s &= U_s e^{j\omega_0 t} \\ \bar{i}_r e^{j\theta} &= i_r(t)e^{j(\theta+\xi)} \end{aligned} \tag{3.11}$$

With collaboration of (3.10) and (3.11),

$$T_s \frac{d}{dt}\left(i_{ms}(t)e^{j\mu}\right) + i_{ms}(t)e^{j\mu} = \frac{1+\sigma_s}{R_s}U_s e^{j\omega_0 t} + i_r(t)e^{j(\theta+\xi)}$$

$$\left(T_s \frac{di_{ms}}{dt} + i_{ms}\right) + j\left(T_s i_{ms}\frac{d\mu}{dt}\right) = \frac{1+\sigma_s}{R_s}\underbrace{U_s e^{j(\omega_0 t-\mu)}}_{u_{sd}+ju_{sq}} + \underbrace{i_r(t)e^{j(\theta+\xi-\mu)}}_{i_{rd}+ji_{rq}}$$

Splitting real and imaginery parts,

$$T_s \frac{di_{ms}}{dt} + i_{ms} = \frac{1+\sigma_s}{R_s}u_{sd} + i_{rd} \tag{3.12}$$

$$T_s i_{ms}\frac{d\mu}{dt} = \frac{1+\sigma_s}{R_s}u_{sq} + i_{rq}$$

and rotation speed of field coordinates (ω_{ms}) becomes

$$\frac{d\mu}{dt} = \frac{1}{T_s i_{ms}}\left[\frac{1+\sigma_s}{R_s}u_{sq} + i_{rq}\right] = \omega_{ms} \tag{3.13}$$

where $u_{sd} = \frac{3\sqrt{2}}{2} U_s \cos(\omega_0 t - \mu)$ and $u_{sq} = \frac{3\sqrt{2}}{2} U_s \sin(\omega_0 t - \mu)$ (Figure 3.6).

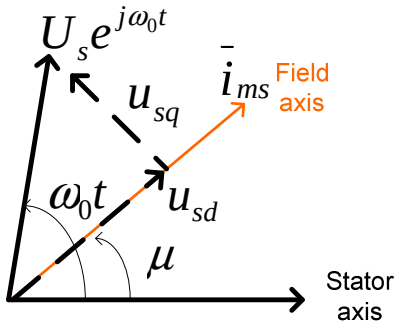

Figure 3.6. Projection of stator voltage vector into field axis

Block representation of i_{ms} and ω_{ms} calculations is depicted in Figure 3.7 using (3.12) and (3.13).

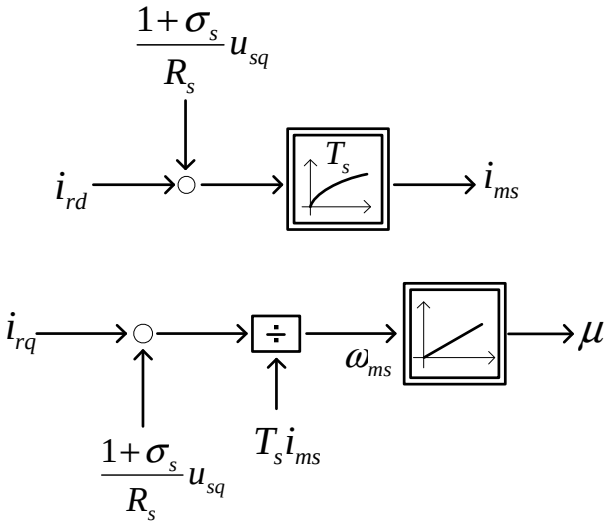

Figure 3.7. i_{ms} and μ calculation

For the sake of simplicity, active and reactive stator currents can be determined in terms of d and q components of rotor current under steady state condition.

$$\bar{u}_s = \frac{3\sqrt{2}}{2} U_s e^{j\omega_0 t}, \quad \bar{i}_s = \frac{3\sqrt{2}}{2} \bar{I}_s e^{j\omega_0 t}, \quad \bar{i}_r e^{j\theta} = \frac{3\sqrt{2}}{2} \bar{I}_r e^{j(\omega+\omega_2)t} = \frac{3\sqrt{2}}{2} \bar{I}_r e^{j\omega_0 t}$$

where $\omega_2 = \dfrac{d\xi}{dt}$ is the frequency of injected rotor current, $\omega_0 = \omega + \omega_2$, $\bar{I}_s = I_s e^{j\varphi_s}$ and $\bar{I}_r = I_r e^{j\varphi_r}$. If equation (3.9) is written in stator coordinates for steady state, stator voltage equation is modified as following

$$\frac{3\sqrt{2}}{2}U_s e^{j\omega_0 t} = R_s \frac{3\sqrt{2}}{2}\bar{I}_s e^{j\omega_0 t} + L_0 \frac{d}{dt}\left[(1+\sigma_s)\frac{3\sqrt{2}}{2}\bar{I}_s e^{j\omega_0 t} + \frac{3\sqrt{2}}{2}\bar{I}_r e^{j\omega_0 t}\right]$$

since $\dfrac{d\bar{I}_s}{dt} = 0$ at steady state, line-to-neutral rms voltage becomes

$$U_s = R_s \bar{I}_s + j\omega_0(1+\sigma_s)L_0\bar{I}_s + j\omega_0 L_0 \bar{I}_r \tag{3.14}$$

When the same procedure is applied for the rotor voltage equation, steady state equivalent circuit is realized as shown in Figure 3.8.

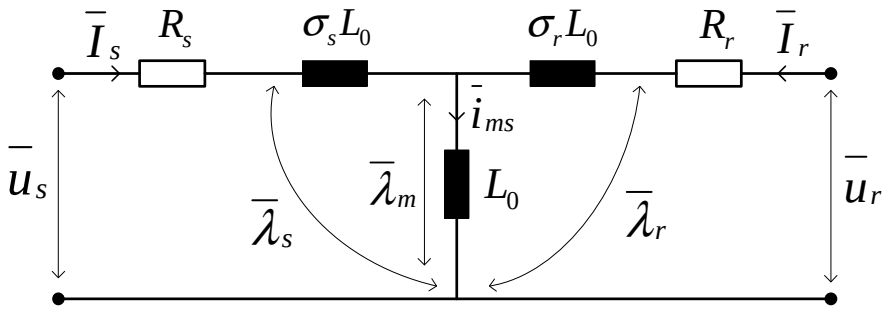

Figure 3.8. Steady state equivalent circuit of doubly-fed induction machine

Stator resistance R_s can be neglected when compared with the impedance of winding inductances especially for high rated machines. Therefore, equation (3.14) is approximated as

$$U_s \cong j\omega_0(1+\sigma_s)L_0\bar{I}_s + j\omega_0 L_0 \bar{I}_r = j\omega_0 L_0 \underbrace{\left[(1+\sigma_s)\bar{I}_s + \bar{I}_r\right]}_{\bar{I}_{ms}}$$

$$\bar{I}_{ms} \cong \frac{U_s}{j\omega_0 L_0} \tag{3.15}$$

When stator flux or equivalently stator magnetizing current is chosen as reference frame and located in the d direct axis, the quadrature component of $\bar{I}_{ms}$ becomes zero.

$$I_{ms} = (1+\sigma_s) i_{sd} + i_{rd} \quad \text{and} \quad 0 = (1+\sigma_s) i_{sq} + i_{rq} \tag{3.16}$$

According to (3.15) and (3.16), the stator magnetizing current is constant along the d axis, and depends on i_{sd}, i_{rd}. If i_{sd} is desired to be comedown for the reactive power, it requires to make i_{rd} increased at the same amount of value. The second equation in (3.16) appears as a constraint for field orientation hence the desired i_{sq} that will be determined from the desired active power is controlled via i_{rq} (Figure 3.9).

Since we are interested in stator current in terms of rotor currents at steady state,

$$\bar{I}_s \cong \frac{1}{j\omega_0(1+\sigma_s)L_0} U_s - \frac{1}{1+\sigma_s} \bar{I}_r = \underbrace{\frac{U_s}{j\omega_0(1+\sigma_s)L_0}}_{\overline{M}} \left(1 - \frac{\bar{I}_r}{\frac{U_s}{j\omega_0 L_0}} \right)$$

$$\bar{I}_s \cong \overline{M}\left(1 - \frac{\bar{I}_r}{\bar{I}_{ms}}\right) = \overline{M}\left(1 - \frac{I_r e^{j(\theta+\xi)}}{I_{ms} e^{j\mu}}\right) = \overline{M}\left(1 - \frac{I_r e^{j\delta}}{I_{ms}}\right)$$

where the vector $\overline{M}$ has constant magnitude and is perpendicular to reference $\bar{u}_s = U_s$. In field coordinates,

$$\bar{I}_s = I_s e^{j\varphi_s} = I_s \cos\varphi_s + jI_s \sin\varphi_s \cong \overline{M}\left(1 - \frac{I_{rd}}{I_{ms}} - j\frac{I_{rq}}{I_{ms}}\right) \tag{3.17}$$

$$I_s \cos\varphi_s \cong -|M|\frac{I_{rq}}{I_{ms}} \quad \text{and} \quad I_s \sin\varphi_s \cong -|M|\left(1 - \frac{I_{rd}}{I_{ms}}\right) \tag{3.18}$$

but equation (3.18) is valid under the following assumptions:

- Stator resistance R_s is neglected

- Steady state operation is considered ($\frac{d\bar{I}_s}{dt} = 0$)

The related phasor representation is depicted in Figure 3.9 for the motor operation.

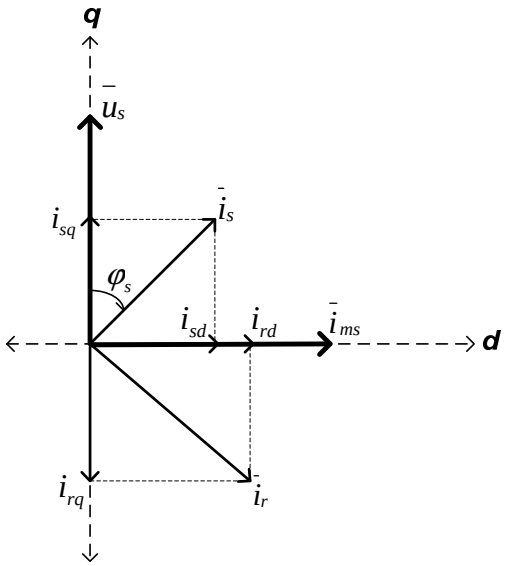

Figure 3.9. The stator and rotor current phasors in field coordinates for motor operation

As observed from Figure 3.9 and using equations (3.17), (3.18), d and q components of stator current are written as

$$I_s \cos\varphi_s = i_{sq}, \text{ and } I_s \sin\varphi_s = i_{sd}$$

Finally, active and reactive powers can be derived as follows

$$P_s = 3\left(\bar{u}_s \bullet \bar{i}_s\right) = 3U_s I_s \cos\varphi_s \cong -\frac{3}{2} U_s |M| \frac{I_{rq}}{I_{ms}} \tag{3.19}$$

$$Q_s = 3\left(\bar{u}_s \times \bar{i}_s\right) = 3U_s I_s \sin\varphi_s \cong \frac{3}{2} U_s |M| \left(\frac{I_{rd}}{I_{ms}} - 1 \right) \tag{3.20}$$

3.2 Simulation Results

Doubly-fed induction machine dynamic model is required to validate the field orientation and orthogonal control of stator current. The first-order electrical and mechanical dynamic equations derived in Chapter 2 are employed in Simulink for open-loop system dynamics. For the sake of simplicity, electrical equations are transformed to rotor coordinates in such a way that slip terms are removed in (2.45) and (2.46).

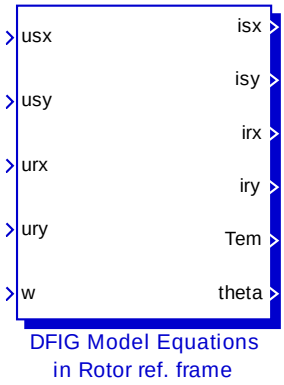

Figure 3.10. Doubly-fed induction machine model in rotor coordinates

When rotor voltages are set to zero in the model, doubly-fed induction machine becomes equivalent to squirrel-cage induction machine. Figure 3.11 verifies the torque-speed characteristics of the squirrel-cage induction machine.

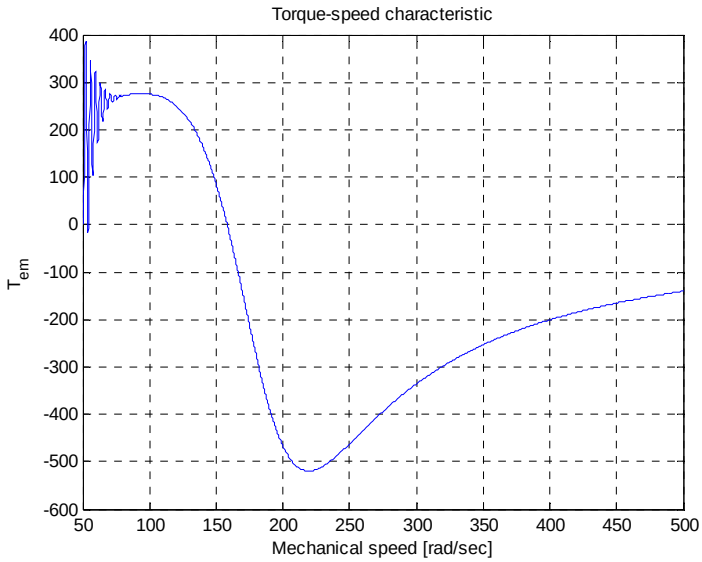

Figure 3.11. The torque-speed characteristics of squirrel-cage IM

The orthogonal control of stator current is observed in the following sections using a simple proportional gain without any stability and tracking analysis. The proportional gain is set to high value. Accordingly the rise time and error signal between actual and reference rotor currents are kept small enough. The rotor current controller, doubly-fed induction machine model (plant) are together shown in Figure 3.12.

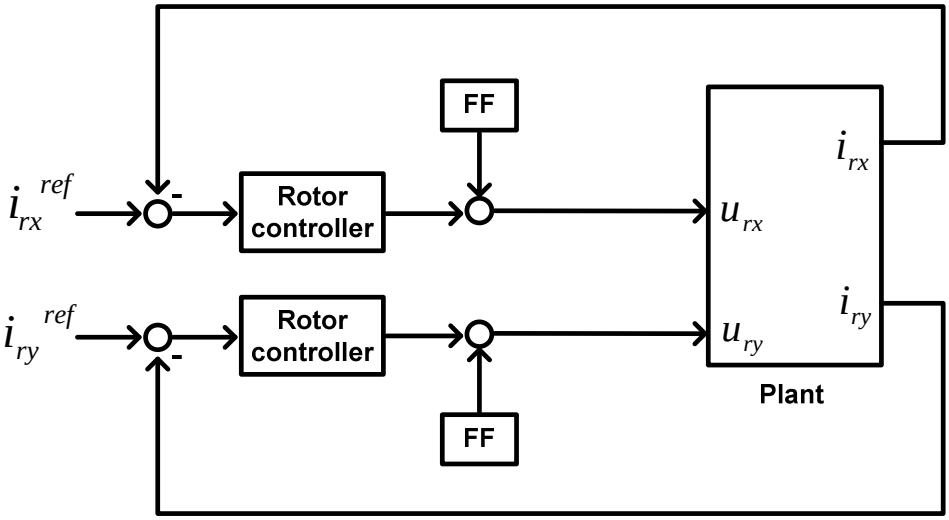

Figure 3.12. Rotor current controller structure with feedforward terms

Using equation (3.16), the rotor voltages can be written in terms of the magnetizing current instead of stator current.

$$L_0 I_{ms} = (1+\sigma_s) i_{sd} + i_{rd} \quad \rightarrow \quad i_{sd} = \frac{L_0}{L_s}(I_{ms} - i_{rd}) \tag{3.21}$$

$$0 = (1+\sigma_s) i_{sq} + i_{rq} \quad \rightarrow \quad i_{sq} = -\frac{L_0}{L_s} i_{rq} \tag{3.22}$$

If (3.21) and (3.22) are inserted into rotor voltages in field coordinates,

$$
\begin{aligned}
u_{rd} &= R_r i_{rd} + L_r \frac{di_{rd}}{dt} + L_0 \frac{di_{sd}}{dt} - (\omega_s - \omega)\left(L_r i_{rq} + L_0 i_{sq}\right) \\
A\frac{di_{rd}}{dt} + i_{rd} &= \frac{1}{R_r} u_{rd} + \left(\omega_{slip} A\right) i_{rq} - B\frac{dI_{ms}}{dt}
\end{aligned}
\tag{3.23}
$$

$$
\begin{aligned}
u_{rq} &= R_r i_{rq} + L_r \frac{di_{rq}}{dt} + L_0 \frac{di_{sq}}{dt} + (\omega_s - \omega)\left(L_r i_{rd} + L_0 i_{sd}\right) \\
A\frac{di_{rq}}{dt} + i_{rq} &= \frac{1}{R_r} u_{rq} - \left(\omega_{slip} A\right) i_{rd} - \left(\omega_{slip} B\right) I_{ms}
\end{aligned}
\tag{3.24}
$$

where $A = \left(L_r - \frac{{L_0}^2}{L_s}\right)\frac{1}{R_r}$ and $B = \frac{{L_0}^2}{R_r L_s}$. Finally, the rotor currents are as follows

$$
\frac{di_{rd}}{dt} = \underbrace{\frac{1}{R_r A}}_{m} u_{rd} + \underbrace{(\omega_s - \omega) i_{rq} - \frac{1}{A} i_{rd} - \frac{B}{A}\frac{dI_{ms}}{dt}}_{f_d} \quad \rightarrow \quad \frac{di_{rd}}{dt} = f_d + m u_{rd} \tag{3.25}
$$

$$
\frac{di_{rq}}{dt} = \underbrace{\frac{1}{R_r A}}_{m} u_{rq} - \frac{1}{A} i_{rq} \underbrace{- (\omega_s - \omega) i_{rd} - (\omega_s - \omega)\frac{B}{A} I_{ms}}_{f_q} \quad \rightarrow \quad \frac{di_{rq}}{dt} = f_q + m u_{rq} \tag{3.26}
$$

f_d and f_q are feedforward terms in (3.25)-(3.26). If the control inputs u_r are selected in such a way that feedforward terms are removed in dynamics, and rotor current errors are defined as $\Delta i_{rd} = {i_{rd}}^{ref} - i_{rd}$, $\Delta i_{rq} = {i_{rq}}^{ref} - i_{rq}$, then simple proportional controller can be designed considering steady state condition ($\dot{i}_{rd}^{\,ref} = 0$, $\dot{i}_{rq}^{\,ref} = 0$). Since the rotor current error dynamics are desired to decrease to zero exponentially,

$$
\Delta \dot{i}_{rd} = \dot{i}_{rd}^{\,ref} - \dot{i}_{rd} = -\dot{i}_{rd} = f_d + m u_{rd}
$$

$$u_{rd} = -\frac{1}{m} f_d - \frac{\lambda_d}{m} \Delta i_{rd} \quad \rightarrow \quad \Delta \dot{i}_{rd} = \lambda_d \Delta i_{rd}, \;\; \lambda_d \in R, \lambda_d > 0 \qquad (3.27)$$

$$\Delta \dot{i}_{rq} = \dot{i}_{rq}^{\,ref} - \dot{i}_{rq} = -\dot{i}_{rq} = f_q + m u_{rq}$$

$$u_{rq} = -\frac{1}{m} f_q - \frac{\lambda_q}{m} \Delta i_{rq} \quad \rightarrow \quad \Delta \dot{i}_{rq} = \lambda_q \Delta i_{rq}, \quad \lambda_q \in R, \lambda_q > 0 \qquad (3.28)$$

Under steady state condition, $\frac{dI_{ms}}{dt} = 0$ in the feedforward term f_d since stator terminal is directly connected to grid.

$$u_{rd} = -\frac{1}{m}\left\{(\omega_s - \omega) i_{rq} - \frac{1}{A} i_{rd}\right\} + K_p \Delta i_{rd}$$
$$u_{rq} = \frac{1}{m}\left\{\frac{1}{A} i_{rq} + (\omega_s - \omega) i_{rd} + (\omega_s - \omega)\frac{B}{A} I_{ms}\right\} + K_p \Delta i_{rq}$$

Although field orientation is realized, the synchronous speed (ω_s) is inserted to the equations instead of field rotational speed (ω_{ms}). This condition should be emphasized that the field speed is settled down to the synchronous speed after transient stage (see eq. (3.15)). When the rotor current controller structure is simulated, it is seen that current errors indicate sufficient damping for demonstration purpose of orthogonal control of stator current. All assumptions to the this end are included to the simulation. Figure 3.13 shows the simulation result of current controller.

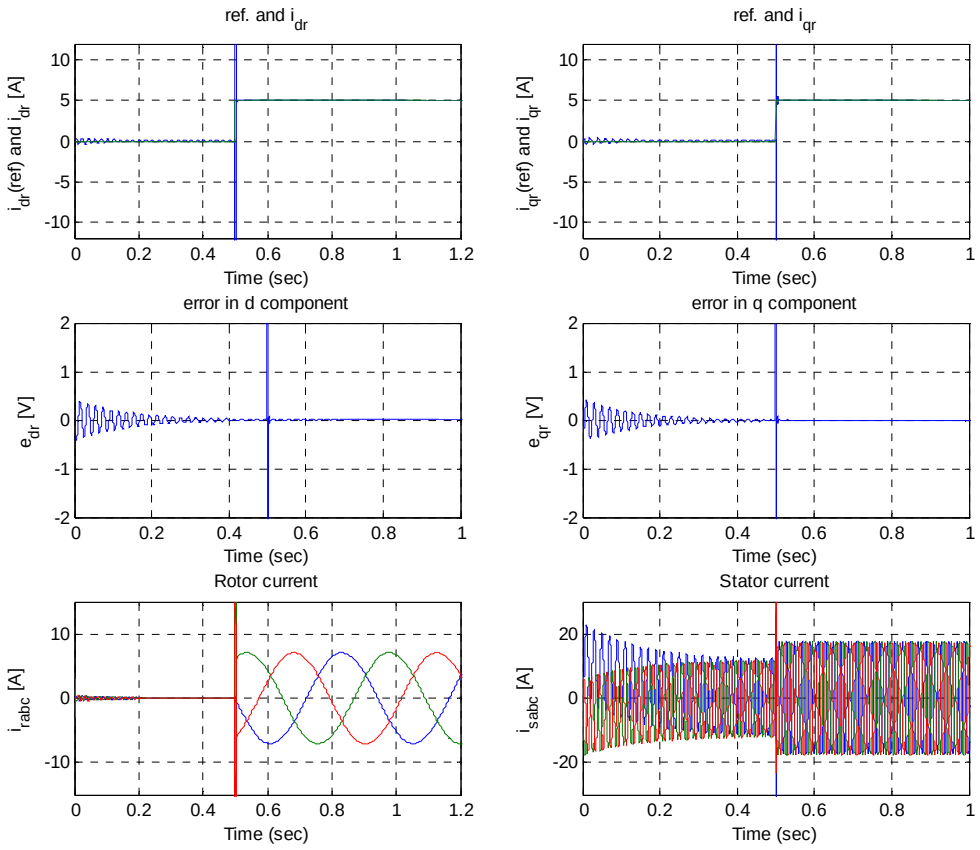

Figure 3.13. Simulation result of current controller (Figure 3.12)

Using the same simulation, the orthogonal control of stator current can be realized. Equations (3.21) and (3.22) are verified as follows:

- Firstly, setting $i_{rd} = 0$, constant value I_{ms} is determined

$$I_{ms} = (1+\sigma_s) i_{sd} + 0 \quad \rightarrow \quad I_{ms} = (1+\sigma_s) i_{sd}$$

- Increase i_{rd} to some positive value and observe how i_{sd} is decreasing to keep I_{ms} constant

- Secondly, observe the relation between the quadrature component of stator current (i_{sq}) and (i_{rq}) using (3.22), $i_{sq} = -\frac{L_0}{L_s} i_{rq}$

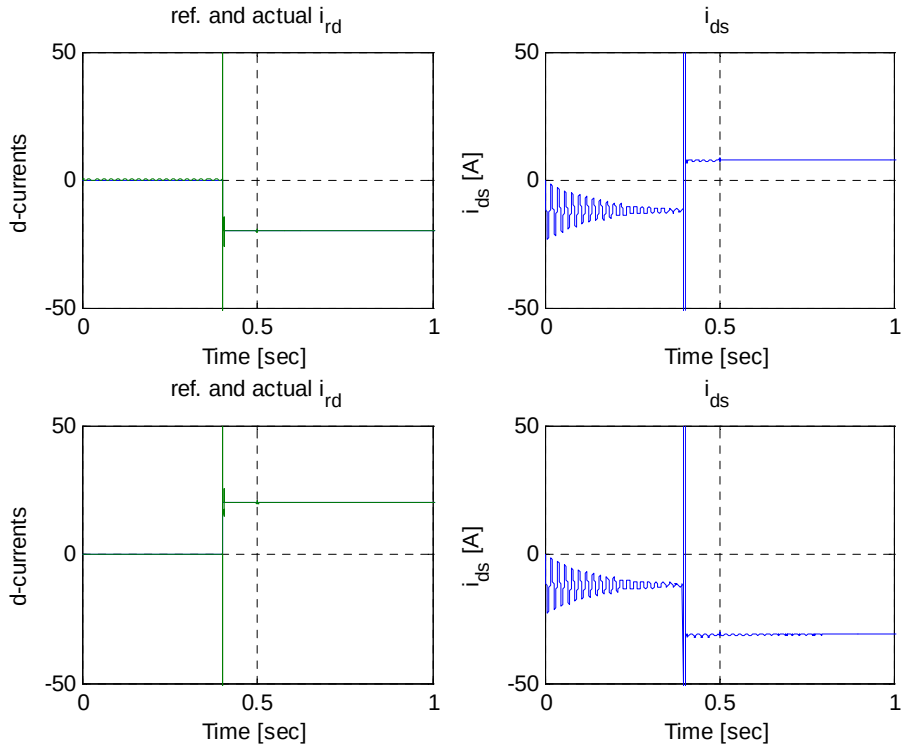

Figure 3.14. Simulation result of control of i_{sd} current

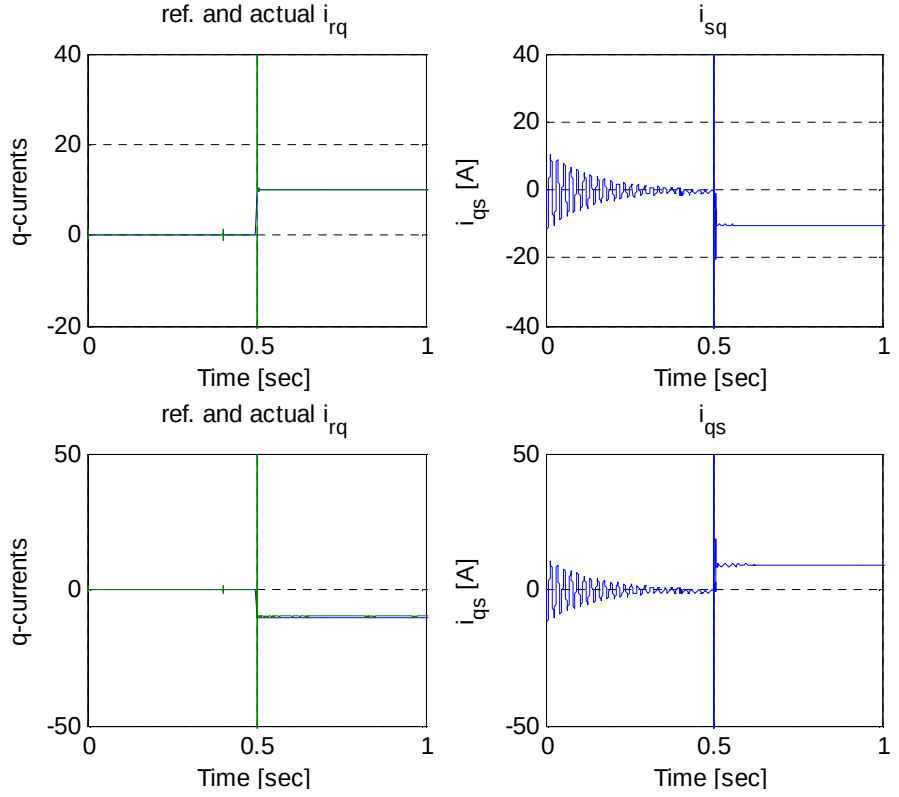

Figure 3.15. Simulation result of i_{sq} current

The orthogonal control of stator current is observed directly from the simulation result depicted in Figure 3.16. Step inputs of rotor currents are given at different time instants to see corresponding stator currents. While i_{sd} is only dependent on i_{rd}, i_{sq} is being controlled via i_{rq} as expected. This condition verifies Figure 3.9 with field orientation.

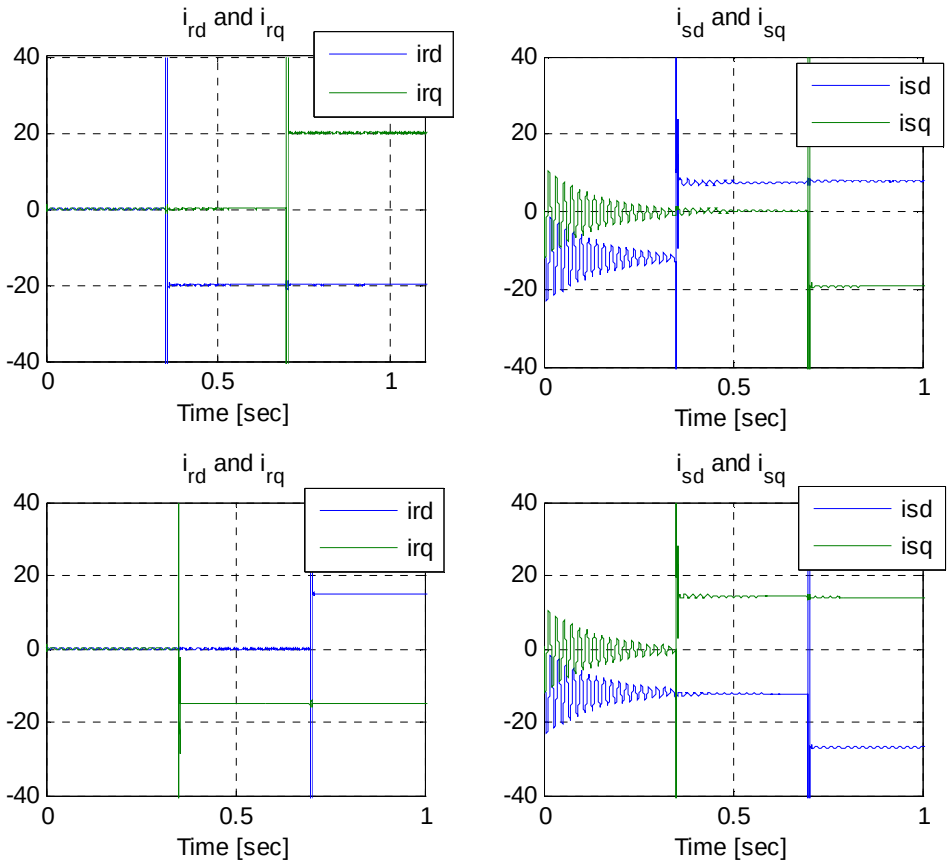

Figure 3.16. Simulation result of orthogonal control of stator current

Both d and q components of stator current can be governed with the related components of rotor current. When active and reactive powers are written in terms of the i_{rd} and i_{rq}, thus decoupling of active and reactive powers is realized. Apparent power can also be written in field coordinates,

$$S = 3\bar{u}_s \bar{i}_s^{\,*} = \frac{3}{2}\left(u_{sd} + ju_{sq}\right)\left(i_{sd} - ji_{sq}\right) = P + jQ$$

$$P = \frac{3}{2}\left(u_{sd} i_{sd} + u_{sq} i_{sq}\right), \text{ and } \quad Q = \frac{3}{2}\left(u_{sq} i_{sd} - u_{sd} i_{sq}\right) \tag{3.29}$$

u_{sd} will converge to zero in stator flux coordinates at steady state because the rotational speed of the synchronous coordinates (ω_s) will be equal to the rotational speed of the stator flux coordinates during steady state.

$$P = \frac{3}{2} u_{sq} i_{sq} = -\frac{3}{2} \frac{L_0}{L_0(1+\sigma_s)} U_s i_{rq} = -\frac{3}{2} \frac{1}{1+\sigma_s} U_s i_{rq} \tag{3.30}$$

$$Q = \frac{3}{2} u_{sq} i_{sd} = \frac{3}{2} U_s \frac{1}{1+\sigma_s} (I_{ms} - i_{rd}) \tag{3.31}$$

Block representation of active and reactive powers in terms of rotor current is shown in Figure 3.17.

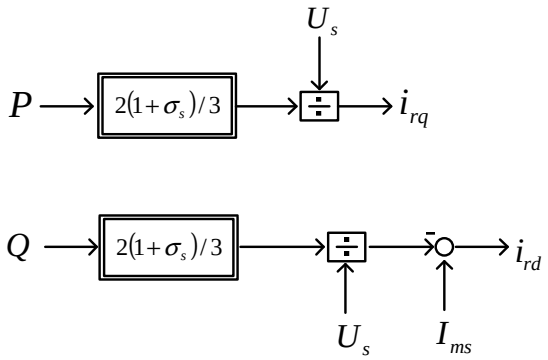

Figure 3.17. Active and reactive powers in terms of rotor current

When the block diagram depicted in Figure 3.17 is added in front of the rotor current controller structure (Figure 3.12), the overall system accomplishes the decoupling of active and reactive powers although any additional controller is not included to Figure 3.17. But feedback term I_{ms} must attract notice in the system.

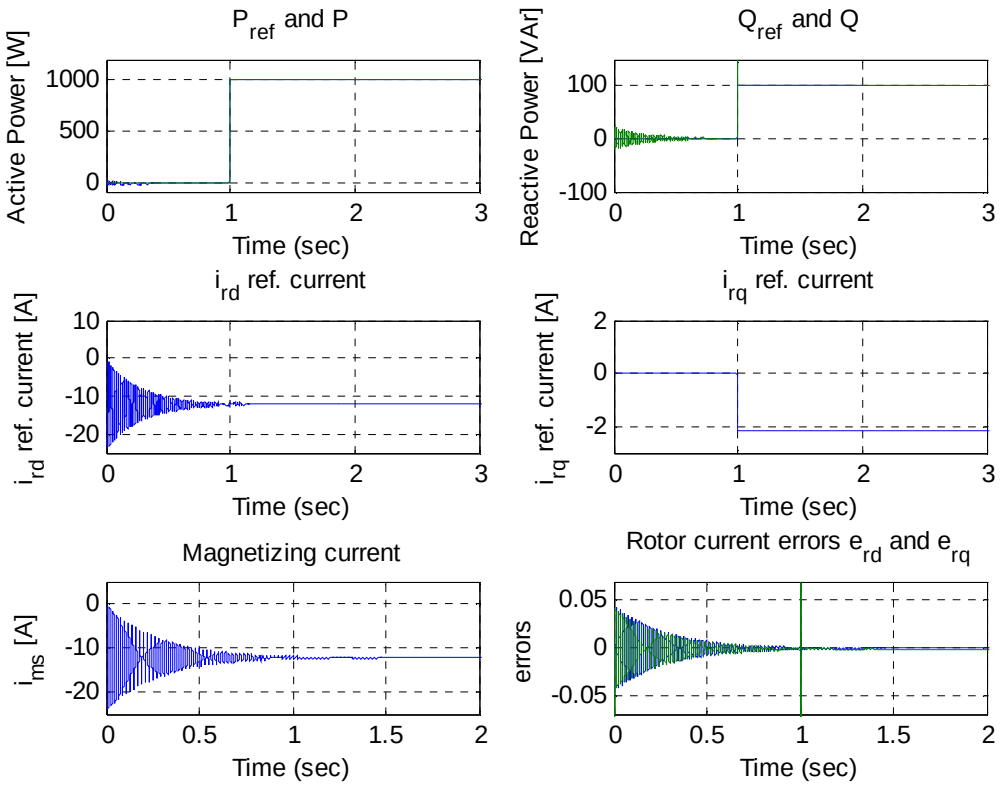

Figure 3.18. Simulation results for decoupling of active and reactive power

As seen from previous figure, actual active and reactive powers can track their references with small amount of steady state errors since only proportional control is realized in rotor current controller and power controller does not exist. The aim was to observe decoupling of active and reactive powers using orthogonal control of stator current and if some drawbacks exist in the structure, then a new approach should be proposed. The d and q components of reference rotor currents generated from Figure 3.17 are depicted in Figure 3.18. Since reference i_{rq} is generated without any feedback term, it does not include any plant dynamics and controller effects. However, the same situation is not valid for reference i_{rd} because of feedback term I_{ms}. According to simulation results shown in Figure 3.18, i_{rd} reference current contains the magnetizing current components. If I_{ms} is not measured or estimated precisely, decoupling of active and reactive powers may become unsuccessful although rotor current controller stabilizes the rotor circuit (equation 3.21).

4 STATOR VOLTAGE-ORIENTED NONLINEAR CONTROL OF ACTIVE AND REACTIVE POWER FLOW BETWEEN DFIM AND GRID

As dictated in the chapter 3, stator flux determination requires exact machine parameters. Any small deviation from exact values is disturbing stator flux orientation, and finally the decoupling of active-reactive power degrades its feasibility. The proposed method described during the chapter overcomes this problem and rotor speed is forced to perceive as disturbance term. The proposed structure is depicted in Figure 4.1. Instead of stator flux orientation, reference frame is oriented with stator voltage which is available for power measurement. Therefore, decoupling of active-reactive power is realized by providing precise measurement of stator voltage.

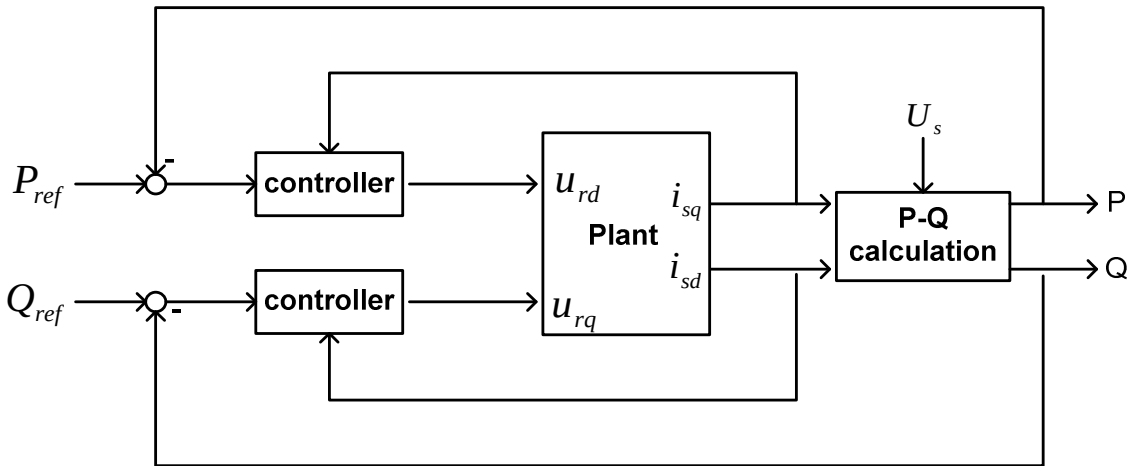

Figure 4.1. Proposed structure for decoupling of active and reactive power

The chapter introduces problem formulation first. Nonlinear controller design and disturbance observer concept are included and the chapter is finalized with simulation results.

4.1 Problem Formulation

When doubly-fed induction machine voltage equations are re-derived in two-phase stator voltage reference frame using equations (3.5), (3.21), and (3.22) under linear magnetic region and balanced conditions,

$$\begin{aligned}
u_{sd} &= R_s i_{sd} + L_s \frac{di_{sd}}{dt} - \omega_s \left(L_s i_{sq} + L_m i_{rq}\right) + L_m \frac{di_{rd}}{dt} \\
u_{sq} &= R_s i_{sq} + L_s \frac{di_{sq}}{dt} + \omega_s \left(L_s i_{sd} + L_m i_{rd}\right) + L_m \frac{di_{rq}}{dt} \\
u_{rd} &= R_r i_{rd} + L_r \frac{di_{rd}}{dt} - \left(\omega_s - \omega\right)\left(L_r i_{rq} + L_m i_{sq}\right) + L_m \frac{di_{sd}}{dt} \\
u_{rq} &= R_r i_{rq} + L_r \frac{di_{rq}}{dt} + \left(\omega_s - \omega\right)\left(L_r i_{rd} + L_m i_{sd}\right) + L_m \frac{di_{sq}}{dt}
\end{aligned} \tag{4.1}$$

where u_{sd}, u_{sq}, u_{rd}, u_{rq} are d-q components of stator and rotor voltages respectively. ω_s, ω are synchronous and rotor electrical speeds. Since stator current dynamics are required for design of nonlinear controller, the related dynamics can be determined as following using equation (4.1),

$$\begin{aligned}
\frac{di_{sd}}{dt} &= -\gamma i_{sd} + \alpha\beta i_{rd} + \beta\omega i_{rq} + \left[\omega_s + \omega(1-\sigma)\right] i_{sq} + \frac{1}{\sigma L_s} u_{sd} - \mu u_{rd} \\
\frac{di_{sq}}{dt} &= -\gamma i_{sq} + \alpha\beta i_{rq} - \beta\omega i_{rd} - \left[\omega_s + \omega(1-\sigma)\right] i_{sd} + \frac{1}{\sigma L_s} u_{sq} - \mu u_{rq}
\end{aligned} \tag{4.2}$$

where $\alpha = \frac{R_r}{L_r}$, $\sigma = L_s\left(1 - \frac{{L_m}^2}{L_s L_r}\right)$, $\beta = \frac{L_m}{\sigma L_s}$, $\gamma = \frac{R_s}{\sigma L_s}$, and $\mu = \frac{L_m}{\sigma L_s L_r}$. The main objective is to track and regulate active-reactive power, therefore, when active and reactive powers are derived as

$$S_s = \frac{3}{2}\bar{u}_s \bar{i}_s = \frac{3}{2}\left(u_{sd} + j u_{sq}\right)\left(i_{sd} + j i_{sq}\right) = P_s + jQ_s$$

$$P_s = \frac{3}{2}\left(u_{sd} i_{sd} + u_{sq} i_{sq}\right)$$
$$Q_s = \frac{3}{2}\left(u_{sq} i_{sd} - u_{sd} i_{sq}\right) \tag{4.3}$$

then the objective can be defined as following

$$\lim_{t\to\infty}\left(P_{ref} - P_s\right) = \lim_{t\to\infty} e_P = 0$$
$$\lim_{t\to\infty}\left(Q_{ref} - Q_s\right) = \lim_{t\to\infty} e_Q = 0 \tag{4.4}$$

where P_{ref} and Q_{ref} are reference active-reactive powers.

4.2 Nonlinear Controller Design

When any dynamical system is generalized as in (4.5), two control objectives are accomplished:

$$\dot{x} = f(x) + u \tag{4.5}$$

- Tracking objective
- Internal stability objective – keeping states bounded

The system defined in (4.5) requires assumptions before controller is accomplished [8].

*Assumption 1: V*ector x is measurable.

Assumption 2: Vector x has solution.

Assumption 3: Given initial value $x(0)$ is bounded.

Assumption 4: If x is bounded, $f(x)$ is also bounded.

Now, error dynamics can be written using equation (4.5) where x_d is defined as desired trajectory or reference input

$$e = x_d - x \quad \rightarrow \quad \dot{e} = \dot{x}_d - \dot{x}$$

$$\dot{e} = \dot{x}_d - f(x) - u \tag{4.6}$$

If control input u is written in such a way that error dynamics solution becomes exponential non-increasing with time (4.8),

$$\dot{e} = -ke \qquad u = -f(x) + \dot{x}_d + ke \tag{4.7}$$

then solution is

$$e(t) = e(0) \bullet e^{-kt} \tag{4.8}$$

where $k > 0$ controller gain. As seen from equation (4.7), control input u calculation needs $f(x)$, $\dot{x}_d$, e information. Since $f(x)$ plant dynamics is difficult task to determine and considered as unknown term for the most dynamical systems, u in (4.7) is applicable only under assumption of known $f(x)$.

In case of doubly-fed induction machine, the active and reactive power error dynamics are

$$\dot{e}_P = \dot{P}_{ref} - \dot{P}_S = \dot{P}_{ref} - \frac{3}{2}\left(\dot{u}_{sd}\, i_{sd} + u_{sd}\, \dot{i}_{sd} \right) - \frac{3}{2}\left(\dot{u}_{sq}\, i_{sq} + u_{sq}\, \dot{i}_{sq} \right)$$

$$\dot{e}_P = F_P - \frac{3}{2}\left(u_{sd}\, \dot{i}_{sd} + u_{sq}\, \dot{i}_{sq} \right) \tag{4.9}$$

$$\dot{e}_Q = \dot{Q}_{ref} - \dot{Q}_S = \dot{Q}_{ref} - \frac{3}{2}\left(\dot{u}_{sq}\, i_{sd} + u_{sq}\, \dot{i}_{sd} - \dot{u}_{sd}\, i_{sq} - u_{sd}\, \dot{i}_{sq} \right)$$

$$\dot{e}_Q = F_Q - \frac{3}{2}\left(u_{sq}\, \dot{i}_{sd} - u_{sd}\, \dot{i}_{sq} \right) \tag{4.10}$$

Inserting equation (4.2) into equation (4.9)-(4.10),

$$\dot{e}_P = F_P - \frac{3}{2}u_{sd}\left[-\gamma i_{sd} + \alpha\beta i_{rd} + \beta\omega i_{rq} + (\omega_s + \omega(1-\sigma))i_{sq} + \frac{1}{\sigma L_s}u_{sd} - \mu u_{rd}\right]$$

$$-\frac{3}{2}u_{sq}\left[-\gamma i_{sq} + \alpha\beta i_{rq} - \beta\omega i_{rd} - (\omega_s + \omega(1-\sigma))i_{sd} + \frac{1}{\sigma L_s}u_{sq} - \mu u_{rq}\right]$$

$$\dot{e}_P = E_P + \frac{3}{2}\mu\left(u_{sd}u_{rd} + u_{sq}u_{rq}\right) \tag{4.11}$$

$$\dot{e}_Q = F_Q - \frac{3}{2}u_{sq}\left[-\gamma i_{sd} + \alpha\beta i_{rd} + \beta\omega i_{rq} + (\omega_s + \omega(1-\sigma))i_{sq} + \frac{1}{\sigma L_s}u_{sd} - \mu u_{rd}\right]$$

$$+\frac{3}{2}u_{sd}\left[-\gamma i_{sq} + \alpha\beta i_{rq} - \beta\omega i_{rd} - (\omega_s + \omega(1-\sigma))i_{sd} + \frac{1}{\sigma L_s}u_{sq} - \mu u_{rq}\right]$$

$$\dot{e}_Q = E_Q + \frac{3}{2}\mu\left(u_{sq}u_{rd} - u_{sd}u_{rq}\right) \tag{4.12}$$

E_P and E_Q terms include doubly-fed induction machine electrical parameters, synchronous and rotor electrical speeds, stator-rotor current and voltages. If these two terms are considered as disturbance and remaining terms in (4.11) and (4.12) are measured directly, u_{rd} and u_{rq} rotor voltages can be selected in such a way that error dynamics solutions decrease exponentially (equation (4.8)).

$$\frac{3}{2}\mu\left(u_{sd}u_{rd} + u_{sq}u_{rq}\right) = -\hat{E}_P - \eta_P e_P \tag{4.13}$$

$$\frac{3}{2}\mu\left(u_{sq}u_{rd} - u_{sd}u_{rq}\right) = -\hat{E}_Q - \eta_Q e_Q \tag{4.14}$$

where η_P and η_Q are positive controller gains for active and reactive power, $\hat{E}_P$ and $\hat{E}_Q$ are estimated active-reactive power disturbances. Inserting (4.13)-(4.14) into (4.11)-(4.12),

$$\dot{e}_P = -\eta_P e_P + \left(E_P - \hat{E}_P\right) \tag{4.15}$$

$$\dot{e}_Q = -\eta_Q e_Q + \left(E_Q - \hat{E}_Q\right) \tag{4.16}$$

The control objective is realized as long as disturbance estimation is accomplished. For this reason, stability analysis is studied under assumption of $\lim_{t\to\infty}\left(E_P - \hat{E}_P\right) = \lim_{t\to\infty}\left(E_Q - \hat{E}_Q\right) = 0$ in equations (4.15)-(4.16). Since stator terminals are connected to grid directly, stator voltages u_{sd}, u_{sq} are known whereas rotor voltages u_{rd}, u_{rq} are selected using equations (4.13) and (4.14).

$$\frac{3}{2}\mu \underbrace{\begin{bmatrix} u_{sd} & u_{sq} \\ u_{sq} & -u_{sd} \end{bmatrix}}_{C} \begin{bmatrix} u_{rd} \\ u_{rq} \end{bmatrix} = \begin{bmatrix} -\hat{E}_P - \eta_P e_P \\ -\hat{E}_Q - \eta_Q e_Q \end{bmatrix}$$

$$\begin{bmatrix} u_{rd} \\ u_{rq} \end{bmatrix} = \frac{2}{3\mu} C^{-1} \begin{bmatrix} -\hat{E}_P - \eta_P e_P \\ -\hat{E}_Q - \eta_Q e_Q \end{bmatrix} \tag{4.17}$$

where

$$C^{-1} = \begin{bmatrix} \dfrac{u_{sd}}{{u_{sd}}^2 + {u_{sq}}^2} & \dfrac{u_{sq}}{{u_{sd}}^2 + {u_{sq}}^2} \\ \dfrac{u_{sq}}{{u_{sd}}^2 + {u_{sq}}^2} & -\dfrac{u_{sd}}{{u_{sd}}^2 + {u_{sq}}^2} \end{bmatrix} = \begin{bmatrix} M & N \\ N & -M \end{bmatrix} \tag{4.18}$$

The inverse of C matrix must be taken into consideration to determine any singular operating condition but as seen from equations (4.17)-(4.18), there is no reason to have singularity except for $\mu = 0$ or $u_{sd} = 0$ and $u_{sq} = 0$ at the same time. Rotor voltages u_{rd} and u_{rq} become

$$u_{rd} = \frac{2}{3\mu}\left[M\left(-\hat{E}_P - \eta_P e_P\right) + N\left(-\hat{E}_Q - \eta_Q e_Q\right)\right] \tag{4.19}$$

$$u_{rq} = \frac{2}{3\mu}\left[N\left(-\hat{E}_P - \eta_P e_P\right) + M\left(\hat{E}_Q + \eta_Q e_Q\right)\right] \tag{4.20}$$

4.3 Stability Analysis

Considering simple positive-definite Lyapunov candidate functions for each error dynamics of active and reactive power,

$$V_P = \frac{1}{2} e_P{}^2 \quad \text{and} \quad V_Q = \frac{1}{2} e_Q{}^2$$

their derivatives can be written as

$$\dot{V}_P = e_P \dot{e}_P = -\eta_P e_P{}^2 \tag{4.21}$$

$$\dot{V}_Q = e_Q \dot{e}_Q = -\eta_Q e_Q{}^2 \tag{4.22}$$

using equations (4.15), (4.16) and under assumption of $\lim_{t\to\infty}\left(E_P - \hat{E}_P\right) = \lim_{t\to\infty}\left(E_Q - \hat{E}_Q\right) = 0$.

According to Asymptotic stability theorem [9], the sufficient and required conditions are as follows for asymptotic stability,

- $V_P(0) = V_Q(0) = 0$
- $V_P > 0$ and $V_Q > 0$
- $\dot{V}_P < 0$ and $\dot{V}_Q < 0$

which satisfies asymptotic stabilitiy of designed controller. To prove that error dynamics solution is global exponentially stable, positive-definite Lyapunov function is written as

$$e_P{}^2 = 2V_P \quad \text{and} \quad e_Q{}^2 = 2V_Q \tag{4.23}$$

and the derivatives of Lyapunov functions can be upper bounded by chosen negative-definite functions

$$\dot{V}_P \le -\eta_P e_P{}^2 \quad \text{and} \quad \dot{V}_Q \le -\eta_Q e_Q{}^2 \tag{4.24}$$

Considering only active power equations and inserting equation (4.23) into (4.24)

$$\dot{V}_P \le -2\eta_P V_P \quad \rightarrow \quad \dot{V}_P + 2\eta_P V_P \le 0 \tag{4.25}$$

If $s(t)$ is defined as a positive function, then equation (4.25) can be modified.

$$\dot{V}_P + 2\eta_P V_P = -s(t)$$

The solution of differential equation is

$$V_P(t) = V_P(0)e^{-2\eta_P t} - \int_0^t e^{-2\eta_P(t-\tau)} s(\tau) d\tau \tag{4.26}$$

Since integral term is always positive, equation (4.26) can be modified to

$$V_P(t) \le V_P(0)e^{-2\eta_P t}$$

$$\frac{1}{2} e_P(t)^2 \le \frac{1}{2} e_P(0)^2 e^{-2\eta_P t} \quad \rightarrow \quad e_P(t) \le e_P(0)e^{-\eta_P t} \tag{4.27}$$

Since P_S and Q_s are bounded provided that their corresponding references are bounded, stator currents i_{sd} and i_{sq} are also bounded from equations 4.3-4.4. To provide internal signals stability, the bounded of rotor voltage, flux, and stator flux signals also must be satisfied

4.4 Disturbance Observer Concept

Stability analysis is valid under $\lim_{t\to\infty}\left(E_P-\hat{E}_P\right)=\lim_{t\to\infty}\left(E_Q-\hat{E}_Q\right)=0$ condition as underlined in previous section. Accordingly, disturbance terms E_P and E_Q are estimated with feasible method [10]. All calculation proceeding for reactive power disturbance observer is the same with active power disturbance observer so only active power related derivations will be considered. Using (4.11),

$$\dot{e}_P = E_P + \frac{3}{2}U_P$$

where $U_P = \mu\left(u_{sd}u_{rd} + u_{sq}u_{rq}\right)$.

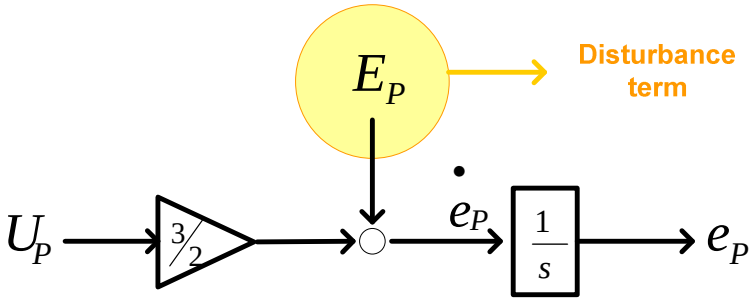

Figure 4.2. Block representation of active power error dynamics

Since objective is to estimate disturbance terms,

$$E_P = \dot{e}_P - \frac{3}{2}U_P$$

the right hand side can be measured through a low pass filter hence estimated disturbance can be written as follows

$$\hat{E}_P = \frac{g}{s+g}\left(\dot{e}_P - \frac{3}{2}U_P\right)$$

$$\hat{E}_P = ge_P - \left(ge_P + \frac{3}{2} U_P \right) \frac{g}{s+g} \tag{4.28}$$

where g is the cut-off frequency or bandwidth of the low-pass filter in radian unit. In electric circuit analogy or built with passive resistor and capacitor elements, g can be selected as

$$g = \frac{1}{RC} = \omega_{cut} \quad \rightarrow \quad f_c = \frac{1}{2\pi fRC}$$

The block representation of active power error dynamics with disturbance observer is depicted in Figure 4.3.

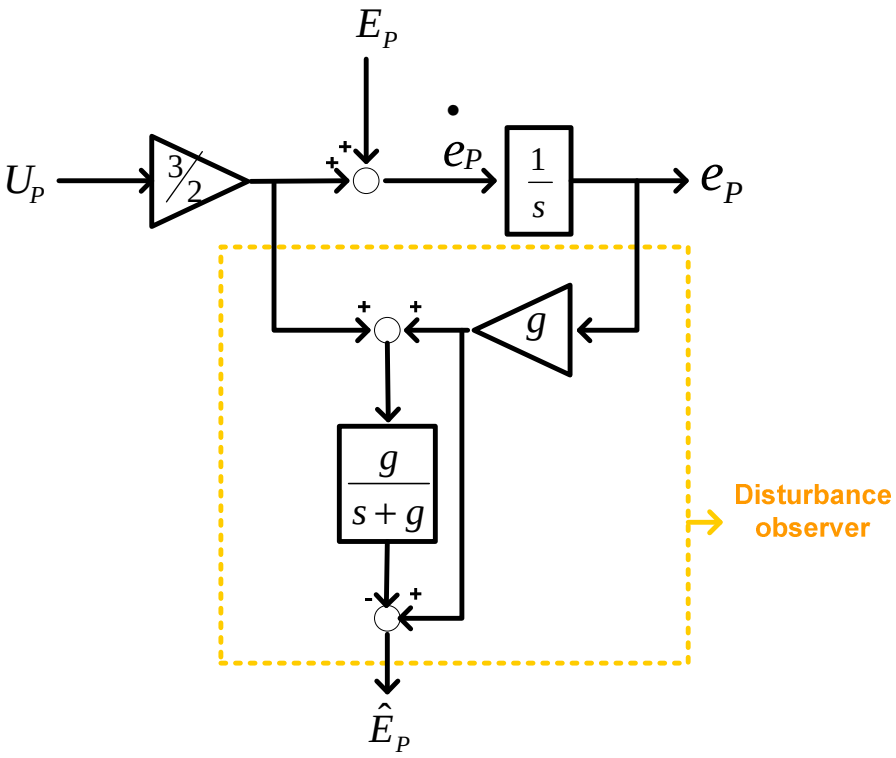

Figure 4.3. The block representation of active power dynamics with disturbance observer

Disturbance estimation is realized by measurable signals like active power for e_P, stator-rotor voltages for U_P (see equation (4.28)). Furthermore, the bandwidth selection capability exists in the system so a convenient bandwidth is used in such a way that

stability which is dictated previous section is kept or $\lim_{t\to\infty}\left(E_P - \hat{E}_P\right) = \lim_{t\to\infty}\left(E_Q - \hat{E}_Q\right) = 0$ condition is reached in finite time.

4.5 Simulation Results

The nameplate of doubly-fed induction machine and additional electrical, mechanical parameters for simulation are shown in Table 4.1 [11].

Table 4.1. DFIM parameters table

Rated power	5	kW
Rated speed	100	rad/sn
Rated voltage	230/380	V
Rated torque	50	Nm
Rated frequency	50	Hz
Rs	0,95	ohm
Ls	0,094	H
Rr	1,8	ohm
Lr	0,088	ohm
Lm	0,082	H
P	3	
J	0,1	kg.m^2

Simulations are realized in two ways:

- Constant rotor speed is applied, and initially reactive power is drawn from utility at 30% of rated power. The desired active and reactive power trajectories are depicted in Figure 4.4.

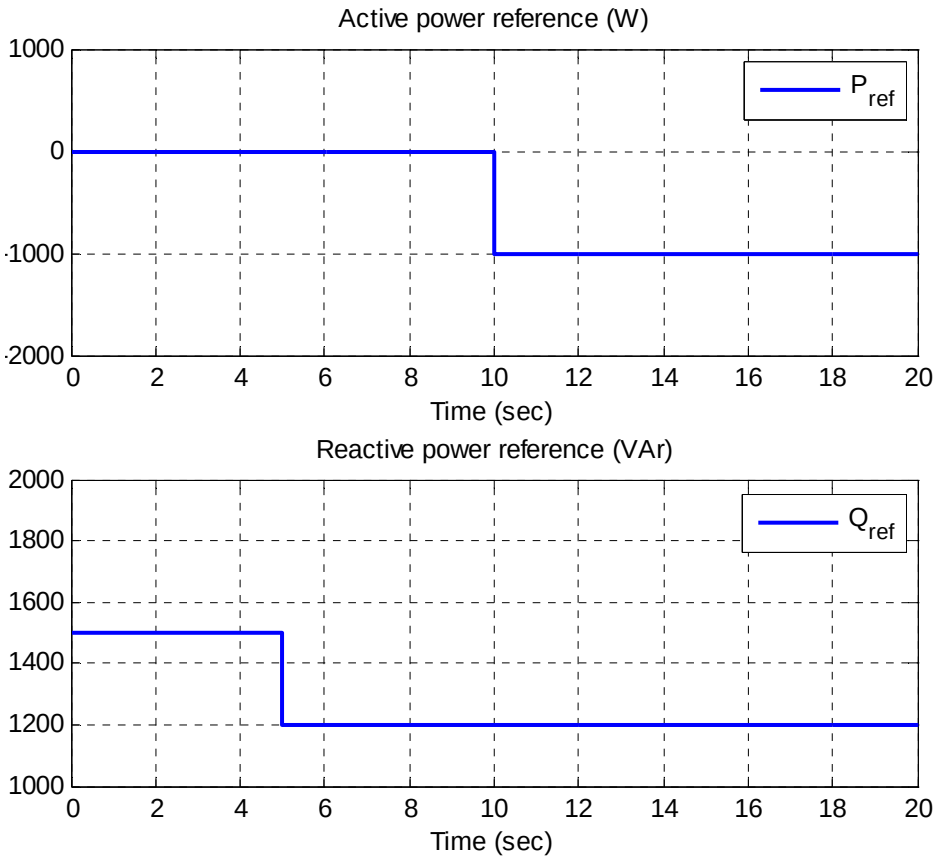

Figure 4.4. Active and reactive power references

Rotor speed is chosen such that slip is near 2%. Therefore, the synchronous speed is

$$n_{sync} = \frac{60f}{P} = \frac{60*50}{3} = 1000 \text{ rpm}$$

where P is the number of poles. The slip speed is calculated as

$$\%slip = \frac{n_{sync} - n}{n_{sync}} * 100$$

$$2 = \frac{1000 - n}{1000} * 100 \quad \rightarrow \quad n = 980 \text{ rpm}$$

The rotor electrical speed in rad/sec is derived as follows

$$\omega_e = \frac{\pi P}{30} n$$

- Since the objective is to control power flow between generator and grid under variable speed, the applied rotor mechanical speed is changed at any time. To observe also sub- and super-synchronous speed operation (under synchronous and over synchronous speed), a rotor mechanical speed reference is given shown in Figure 4.5.

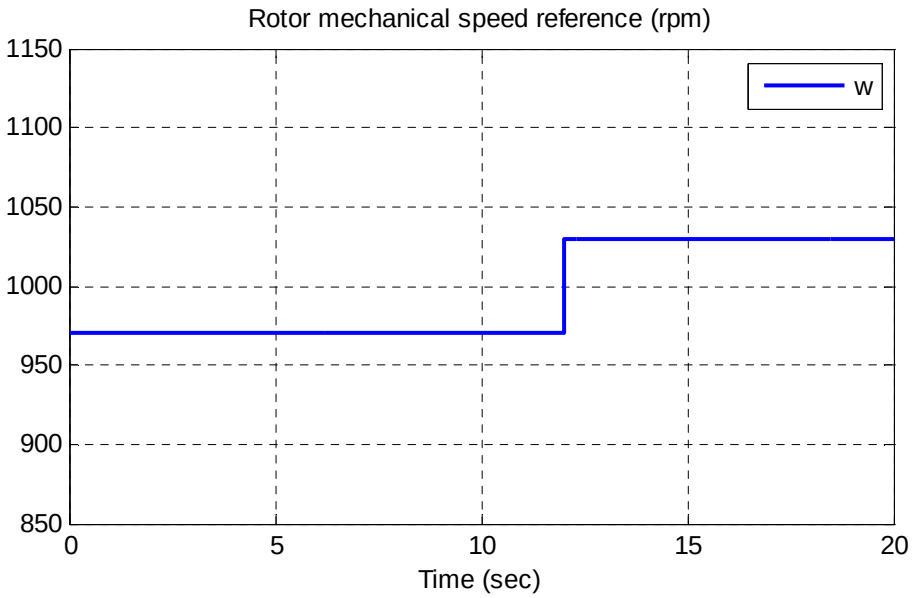

Figure 4.5. The rotor mechanical speed reference

Table 4.2. Controller and simulation constants

Description		Value
Low pass filter cut-off frequency	g	100
Active power controller gain	η_P	200
Reactive power controller gain	η_Q	200
Grid voltage electrical speed (rad/s)	ω_0	100π

Using selected parameters shown in Table 4.2 and keeping these parameters constant during simulation, the results are obtained under constant rotor mechanical speed (2% slip – sub-synchronous) in Figure 4.6.

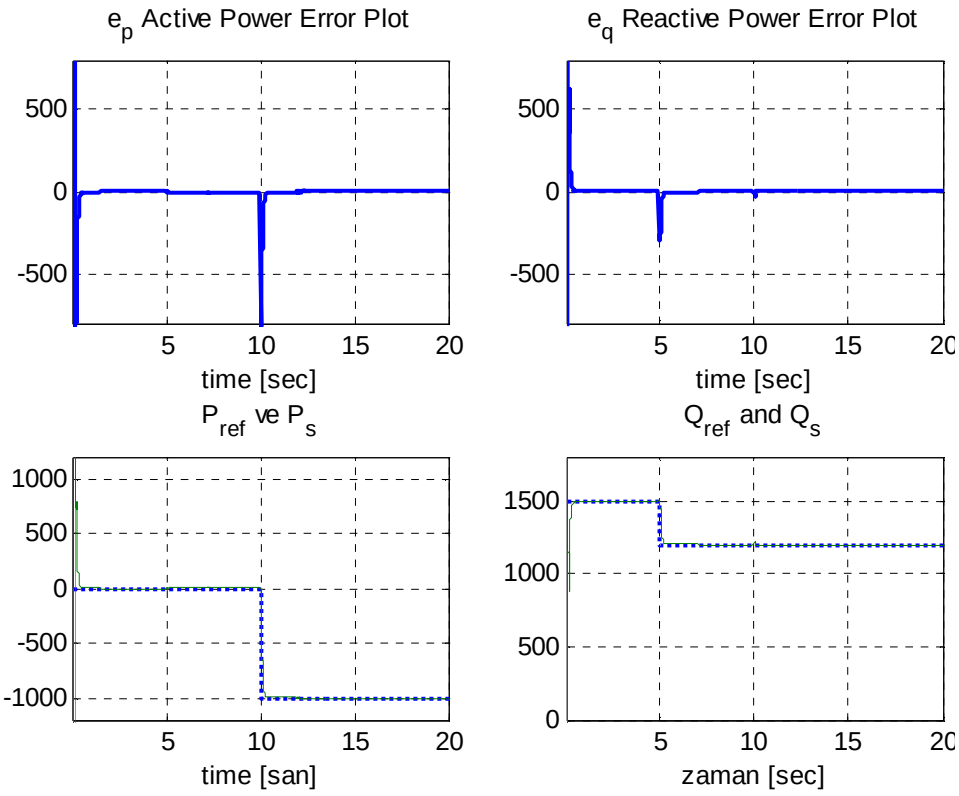

Figure 4.6. Simulation plots of error, active and reactive power under constant rotor speed

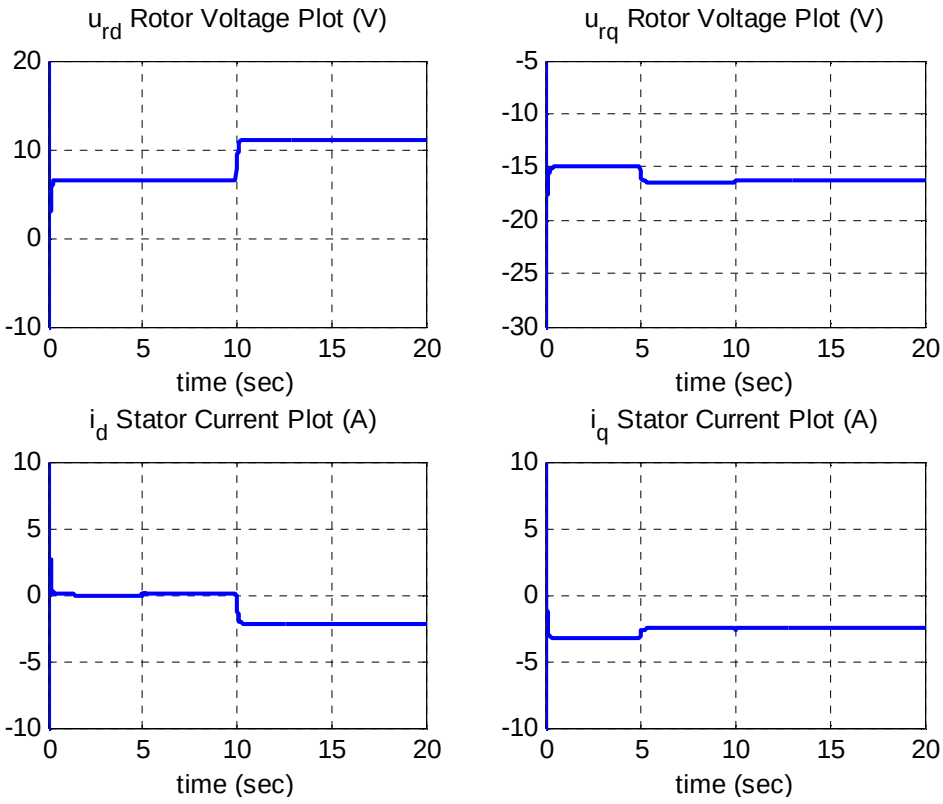

Figure 4.7. Simulation plots of rotor voltage and stator currents in synchronous frame under constant rotor speed

Two results can be figured out from Figure 4.6. The first one is that decoupling of active and reactive power is achieved in grid voltage frame. Reactive power reference does not have influence on active power reference traction. Another result that should be highlighted is tracking performance of the proposed nonlinear controller with disturbance observer as error plots give reasonable results with bounded rotor voltages and stator currents. Since stator voltage is assumed constant, power flow between stator terminals of doubly-fed induction machine and grid depends on stator currents indirectly as verified from Figure 4.7.

Grid-connected operation under variable rotor or turbine mechanical speed is also tested in Matlab Simulink environment. As a step input, rotor speed is changed from 980 rpm to 1020 rpm (Figure 4.5).

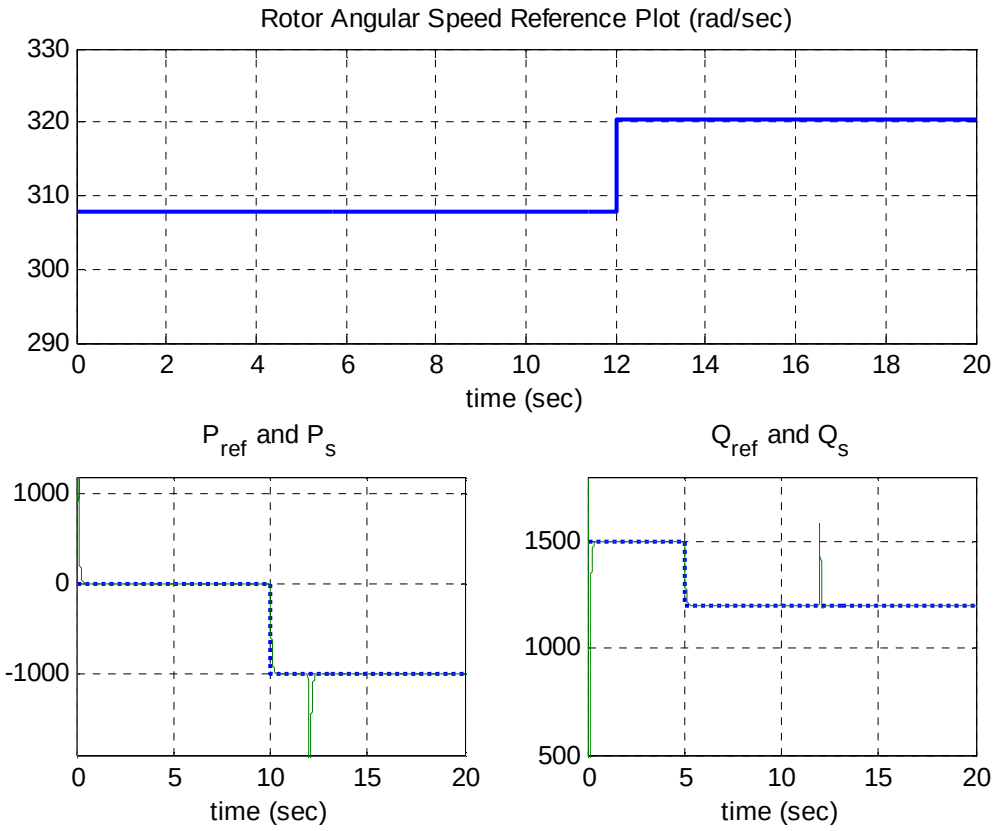

Figure 4.8. Tracking performances of active-reactive power controller under variable rotor speed

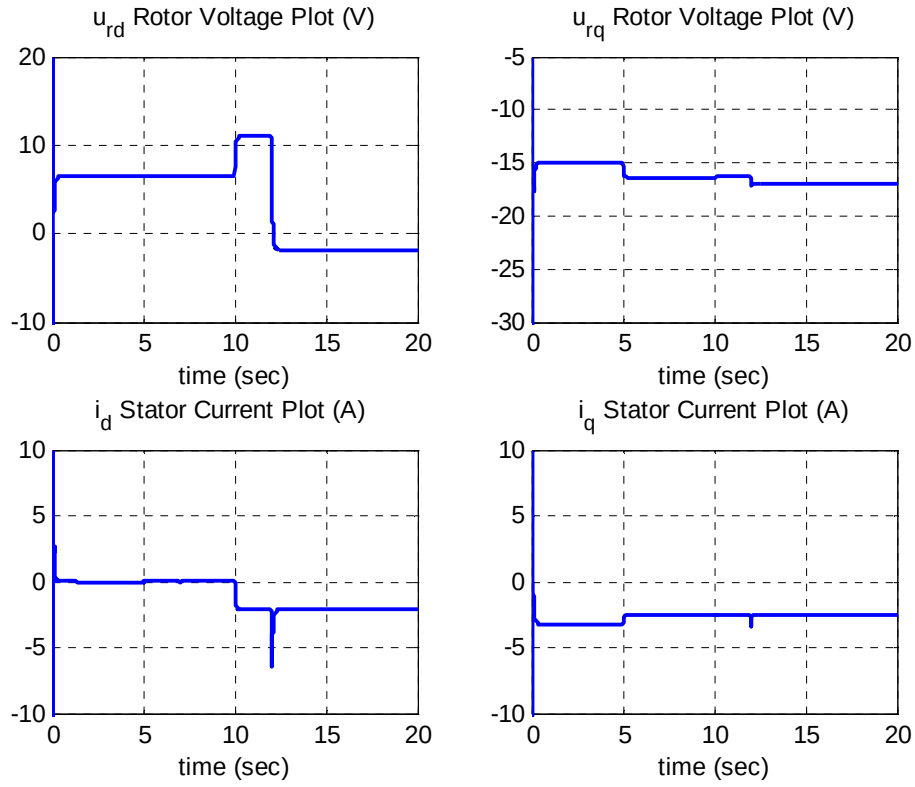

Figure 4.9. Simulation plots of rotor voltage and stator currents in synchronous frame under variable rotor speed

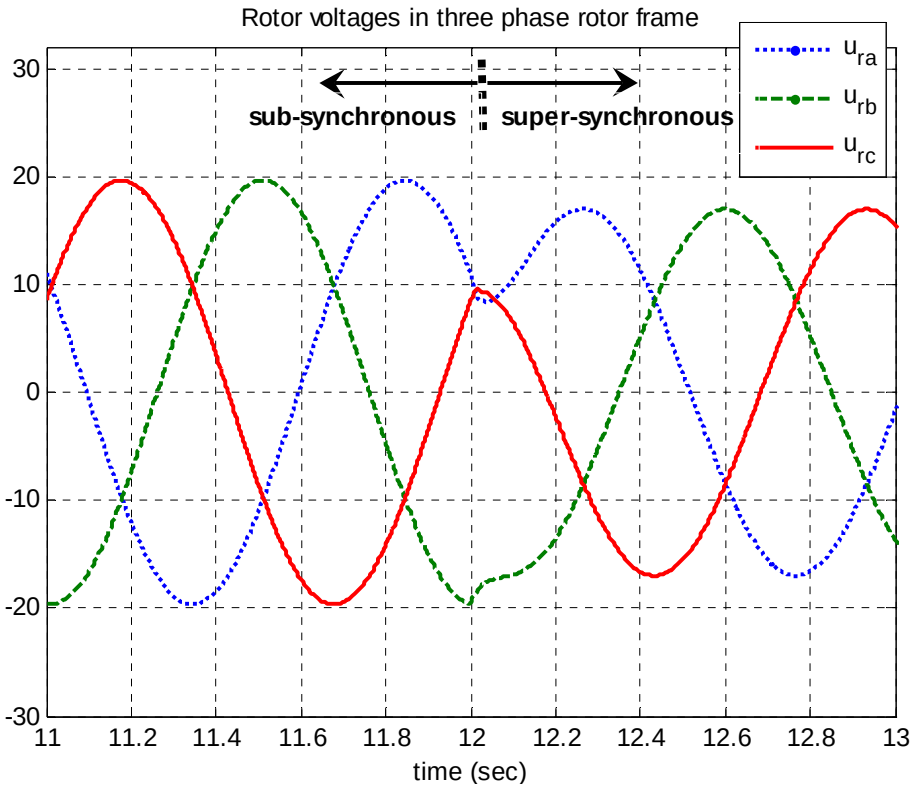

Figure 4.10. Simulation plots of rotor voltages in abc rotor frame under variable rotor speed

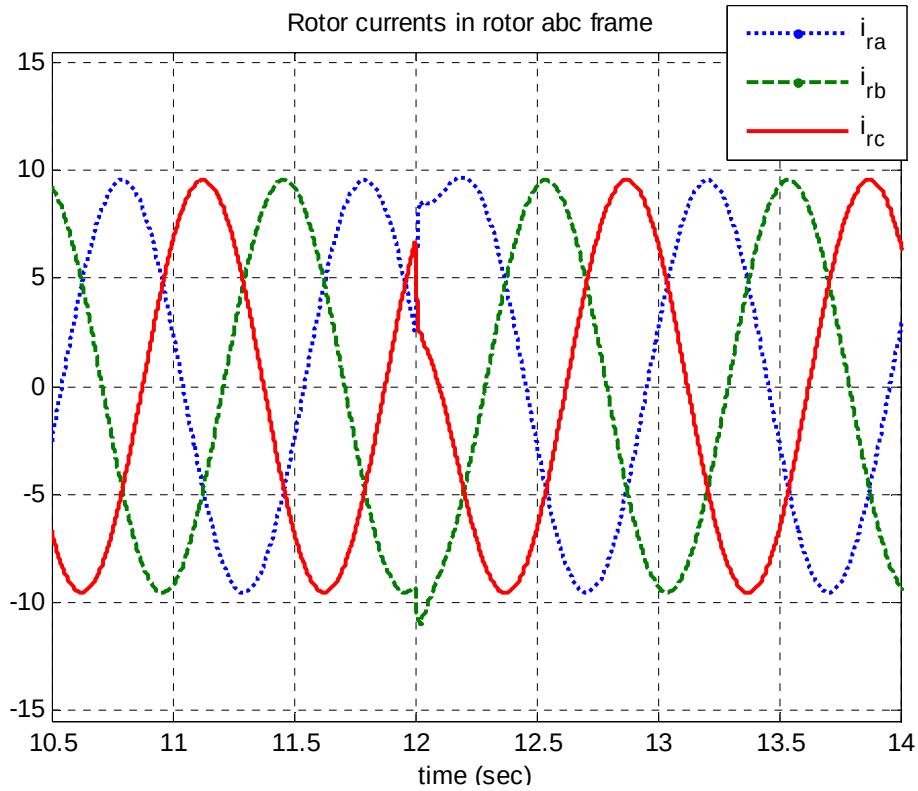

Figure 4.11. Simulation plots of rotor currents in abc rotor frame under variable rotor speed

As seen from Figure 4.8, a rotor speed is changed at 12th second and speed variation effects can be observed. Active-reactive power tracking is still achieved with reasonable rotor voltages and stator currents. Rotor speed is at under synchronous speed initially and then increased to above synchronous speed. After that transition time, rotor voltage/current is in reversed phase (Figure 4.10-4.11) and this condition can be explained using steady-state model of doubly fed induction machine including magnetizing losses [4]. When equations 2.45 and 2.46 are written in more generalized form instead of in terms of x, y components,

$$U_s = R_s I_s + j\omega_s \lambda_s \tag{4.29}$$

$$U_r = R_r I_r + j(\omega_s - \omega)\lambda_r$$

$$\lambda_s = L_s I_s + \lambda_m \tag{4.30}$$

$$\lambda_r = L_r I_r + \lambda_m \tag{4.31}$$

where $\lambda_m = L_m I_m = L_m (I_s + I_r + I_{mR})$ and I_{mR} is magnetizing resistor current. If slip is defined as,

$$s = \frac{\omega_s - \omega}{\omega_s}$$

then rotor voltage in steady state is

$$U_r = R_r I_r + js\omega_s \lambda_r \quad \rightarrow \quad \frac{U_r}{s} = \frac{R_r}{s} I_r + j\omega_s \lambda_r \tag{4.32}$$

Using equations (4.29)-(4.32), steady-state equivalent circuit is formed as shown in 4.12.

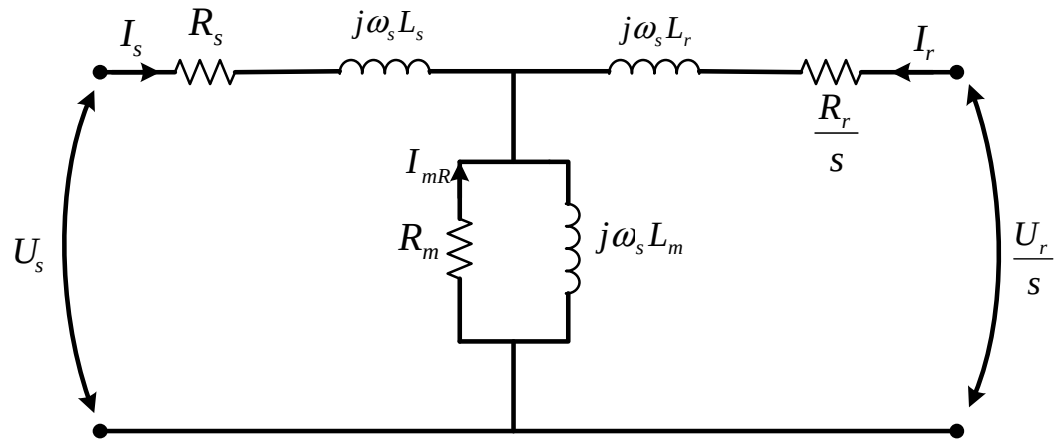

Figure 4.12. Steady-state equivalent circuit of DFIM with magnetizing losses for power flow analysis

The stator apparent power and consequently active-reactive power for both rotor and stator are derived using steady-state model to investigate power flow.

$$S_s = 3U_s I_s^* = 3\left(R_s I_s + j\omega_s \lambda_s\right) I_s^* = 3R_s \left|I_s\right|^2 + j3\omega_s \lambda_s I_s^*$$

Inserting equation (4.30),

$$S_s = 3R_s \left|I_s\right|^2 + j3\omega_s L_s \left|I_s\right|^2 + j3\omega_s \lambda_m I_s^* \tag{4.33}$$

Since voltages are equal to each other for the parallel magnetizing branch in the steady-state equivalent circuit,

$$R_m I_{mR} = -j\omega_s L_m \left(I_s + I_r + I_{mR}\right) = -j\omega_s \lambda_m \tag{4.34}$$

$$I_s = j\frac{R_m}{\omega_s L_m} I_{mR} - I_r - I_{mR} \quad \rightarrow \quad I_s^* = j\frac{R_m}{\omega_s L_m} I_{mR}^* - I_r^* - I_{mR}^*$$

and if equation (4.33) is written in terms of I_r and I_{mR} using equation (4.34),

$$S_s = 3R_s \left|I_s\right|^2 + j3\omega_s L_s \left|I_s\right|^2 + j3\omega_s \lambda_m \left(j\frac{R_m}{\omega_s L_m} I_{mR}^* - I_r^* - I_{mR}^* \right)$$

$$S_s = 3R_s|I_s|^2 + j3\omega_s L_s|I_s|^2 + j3\omega_s \frac{|\lambda_m|^2}{L_m} - j3\omega_s \lambda_m I_r^* + 3R_m|I_{mR}|^2 \quad (4.35)$$

Stator active-reactive power can easily be determined as following

$$P_s = \mathrm{Re}[S_s] = 3R_s|I_s|^2 + 3R_m|I_{mR}|^2 + 3\omega_s \,\mathrm{Im}[\lambda_m I_r^*] \quad (4.36)$$

$$Q_s = \mathrm{Im}[S_s] = 3\omega_s L_s|I_s|^2 + 3\omega_s \frac{|\lambda_m|^2}{L_m} - 3\omega_s \,\mathrm{Re}[\lambda_m I_r^*] \quad (4.37)$$

For the sake of simplicity for power flow analysis, the first two terms which correspond to resistive losses are neglected and equation (4.36) can be approximated as

$$P_s \approx 3\omega_s \,\mathrm{Im}[\lambda_m I_r^*] \quad (4.38)$$

$$Q_s \approx -3\omega_s \,\mathrm{Re}[\lambda_m I_r^*] \quad (4.39)$$

Applying the same procedure for rotor apparent power,

$$S_r = 3U_r I_r^* = 3(R_r I_r + j\omega_s s\lambda_r) I_r^* = 3R_r|I_r|^2 + j3\omega_s s\lambda_r I_r^*$$

Inserting equation (4.31),

$$S_r = 3R_r|I_r|^2 + j3\omega_s sL_r|I_r|^2 + j3\omega_s s\lambda_m I_r^* \quad (4.40)$$

Rotor active and reactive power become as follows

$$P_r = \mathrm{Re}[S_r] = 3R_r|I_r|^2 - 3\omega_s s\,\mathrm{Im}[\lambda_m I_r^*]$$

$$Q_r = \mathrm{Im}[S_r] = 3\omega_s sL_r|I_r|^2 + 3\omega_s s\,\mathrm{Re}[\lambda_m I_r^*]$$

Again after approximations by neglecting loss terms,

$$P_r \approx -3\omega_s s \,\mathrm{Im}\left[\lambda_m I_r^{\,*}\right] \tag{4.41}$$

$$Q_r \approx 3\omega_s s \,\mathrm{Re}\left[\lambda_m I_r^{\,*}\right] \tag{4.42}$$

It is notable to emphasize relationship between stator and rotor active power using equations (4.38) and (4.41),

$$P_r = -sP_s \tag{4.43}$$

Therefore, power flow can be visualized as in Figure 4.13. Since slip is defined as

$$s = \frac{\omega_s - \omega}{\omega_s} = \frac{n_s - n}{n_s}$$

and $P_s < 0$ in generator mode, when mechanical speed passes beyond synchronous speed, slip becomes negative and power is delivered from rotor to grid. On the contrary, power is drawn from grid during sub-synchronous operation. Figure 4.11 and 4.12 depicts the effect of synchronous speed transition at 12th second. As observed from these figures, rotor current direction is reversed.

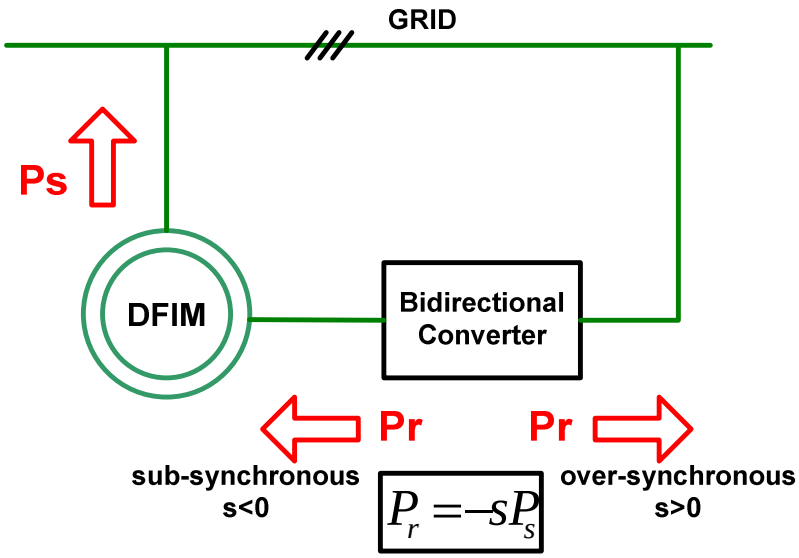

Figure 4.13. Power flow between DFIM and grid

The proposed method should be implementable by feasible measurements. Three main measurements must be realized to implement the method by using voltage and current sensors: Stator voltage, rotor voltage and stator current (active & reactive power measurement).

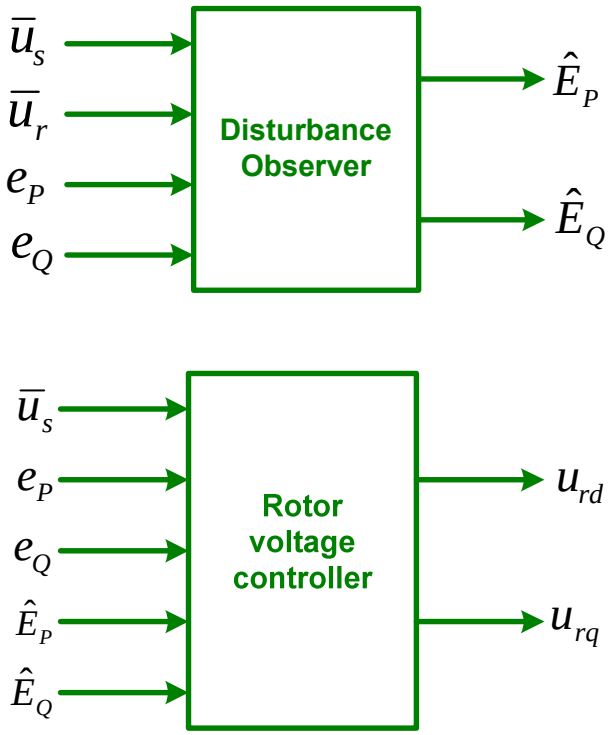

Figure 4.14. Block representations of disturbance observer and rotor voltage controller

5 VOLTAGE SOURCE CONVERTERS

By the time, two approaches which are orthogonal control of active-reactive power with stator flux-orientation and nonlinear control with disturbance observer have been described. Since stator flux orientation requires flux estimation, the orthogonality of active-reactive power depends on this estimation and some assumptions. The proposed method is grid voltage-oriented and only precise grid voltage measurement is essential.

Doubly-fed induction machine can have two operating modes: sub-synchronous mode and super-synchronous mode during generator operation. As mentioned in the chapter 4, rotor power direction changes according to sub- or super-synchronous modes. To have wide rotor speed range, a bi-directional power converter that is connected between rotor and grid is required.

Although improved techniques exist for bi-directional power converters (dc-link capacitor or inductor-free, resonant techniques, etc.), the most widespread used converter is back-to-back converter for bi-directional power flow. Typically, two different approaches are situated at back-to-back converters: Current source converter (CSC) and voltage source converter (VSC). The proposed active-reactive power controller generates rotor voltage reference thus 3-phase voltage source converter should be placed in the system.

A back-to-back converter consists of two voltage source converters and a dc-link capacitor is located between them (Figure 5.1). Each leg of converters provides bi-directional power flow with parallel switching devices and diodes. DC-link capacitor plays a role of energy transfer component as keeping its voltage level constant.

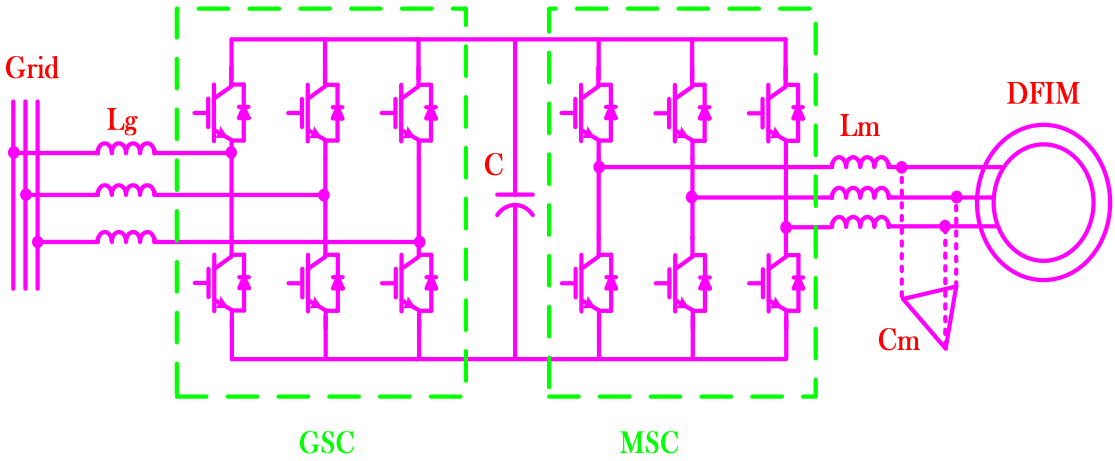

Figure 5.1. Back-to-back converter

Therefore, grid side converter (GSC) is responsible of maintaining dc-link voltage at a certain level. Besides, a unity power factor can be provided at the grid connection at the same time. Orthogonal control of active-reactive power consequently rotor voltages can be generated by machine side converter (MSC).

Only grid side converter is considered in the thesis. The same modeling and control of GSC is also valid for machine side converter.

5.1 Grid Side Converter (Three Phase Boost Converter)

In this section, working principle of grid side converter (GSC) will be investigated. Two main objectives are given to GSC:

- Keep voltage level of dc-link capacitor at a certain value
- Provide unity power factor at grid side

Because of line filter inductors L_G, one leg of GSC can be considered as a boost converter (Figure 5.2) and dc-link voltage is mostly higher than the magnitude of input ac voltage. Accordingly, GSC is called as 3-phase boost rectifier.

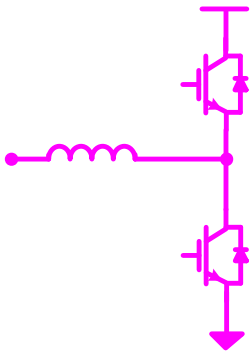

Figure 5.2. One leg of GSC

To investigate operation of GSC, the converter model is derived at first. From control point of view, a nonlinear variable structure system control law is developed using model of GSC.

5.1.1 Modeling of Grid Side Voltage Source Converter

A three-phase converter consists of three poles and each pole has upper and lower switches with assigned parallel diodes (Figure 5.2). Upper and lower switches operate as complementary with negligible deadtime to avoid line short circuit. Therefore, if upper switches are controlled by pulse width modulation (pwm) signals with d_a, d_b, d_c duty cycles that ranges between zero and one,

$$0 \le d_a \le 1$$

then pwm signals with $\bar{d}_a, \bar{d}_b, \bar{d}_c$ duty cycles are applied to lower switches where $\bar{d}_a = 1 - d$.

Then by applying Kirchoff's laws, the mathematical model of circuit depicted in Figure 5.3 can be defined in stationary frame with neglected resistance of inductors as:

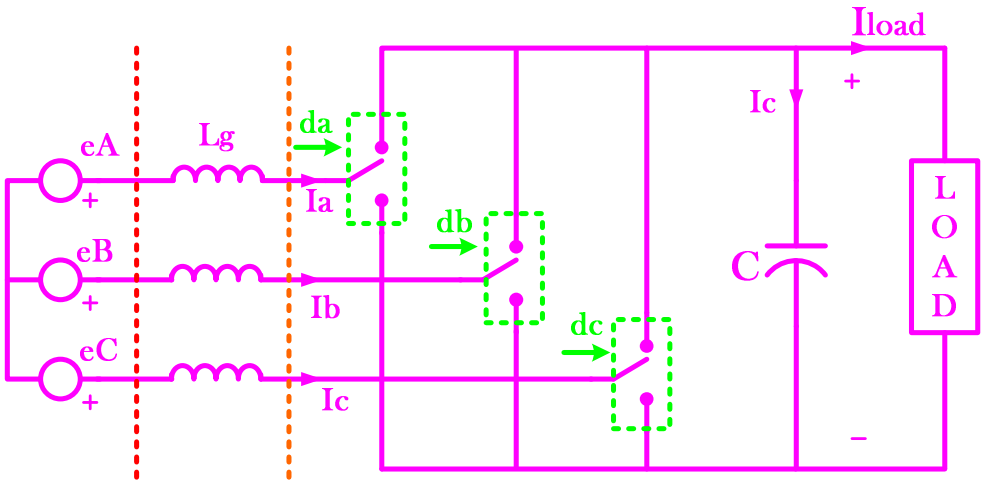

Figure 5.3. 3-phase boost rectifier topology

$$L_g \frac{di_a}{dt} = e_A - d_a V_{DC} \quad \rightarrow \quad \frac{di_a}{dt} = \frac{1}{L_g} e_A - \frac{1}{L_g} d_a V_{DC} \tag{5.1}$$

$$\frac{di_b}{dt} = \frac{1}{L_g} e_B - \frac{1}{L_g} d_b V_{DC} \tag{5.2}$$

$$\frac{di_c}{dt} = \frac{1}{L_g} e_C - \frac{1}{L_g} d_c V_{DC} \tag{5.3}$$

DC-link capacitor voltage equation is as follows:

$$C \frac{dV_{DC}}{dt} = d_a i_a + d_b i_b + d_c i_c - i_{load} \tag{5.4}$$

Equations 5.1-5.4 are derived in stationary frame so the currents i_a, i_b, i_c are sinusoidal quantites. Since output voltage V_{DC} is constant, average of duty cycles d_a, d_b, d_c are also sinusoidal quantities which have same frequency with grid voltage. If stationary frame is rotated with grid voltage speed which means synchronous speed, then currents and duty cycles will be dc quantities. Controller design in synchronous frame will be easier because of dc quantites and equations 5.1-5.4 can be modified to synchronous frame as following

$$\frac{d}{dt}\left(i_d e^{-j\theta_s}\right) = \frac{1}{L_g} e_d e^{-j\theta_s} - \frac{1}{L_g} d_d e^{-j\theta_s} V_{DC} = e^{-j\theta_s} \frac{di_d}{dt} - \omega_s i_q e^{-j\theta_s}$$

$$e_d = Ri_d + L_g \frac{di_d}{dt} + d_d V_{DC} - \omega_s L_g i_q \tag{5.5}$$

$$e_q = Ri_q + L_g \frac{di_q}{dt} + d_q V_{DC} + \omega_s L_g i_d \tag{5.6}$$

$$C \frac{dV_{DC}}{dt} = (d_d i_d + d_q i_q) - i_{load} \tag{5.7}$$

where $\omega_s = 2\pi f$. If d axis of synchronous reference frame is aligned to grid voltage vector (Figure 5.4), then $e_d = \vec{e}$ and $e_q = 0$.

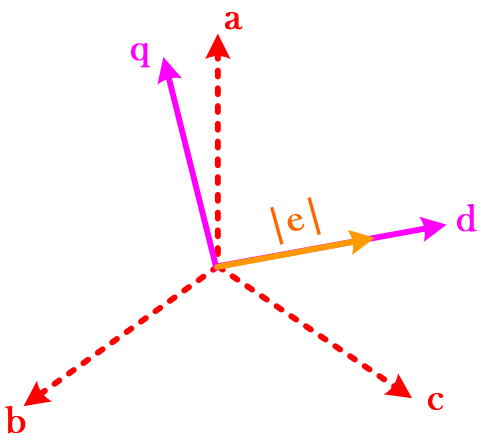

Figure 5.4. Grid orientation

Equations 5.5-5.7 determine average large signal model of grid side converter. Figure 5.5 depicts equivalent circuit of average large signal model of the converter in synchronous frame.

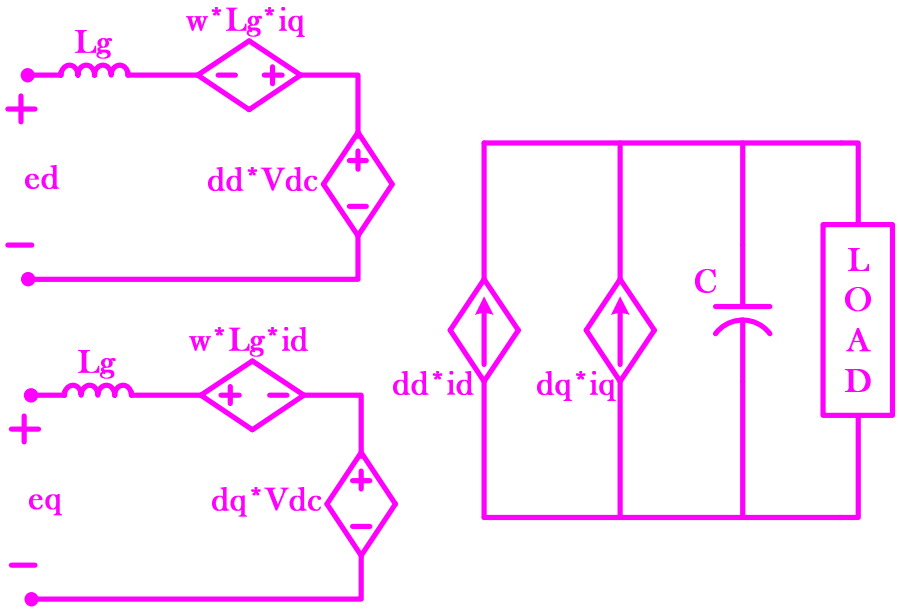

Figure 5.5. Equivalent circuit of average large signal model of GSC

As seen from Figure 5.5, cross terms are added after transformation from stationary frame to synchronous frame. These cross terms make voltage equations nonlinear.

5.1.2 VSS Controller Design

The controller objective is to keep dc-link voltage at a desired level and to provide unity power factor for grid side converter. When reactive power is written in synchronous frame,

$$Q = \frac{3}{2}\left(e_q i_d - e_d i_q\right)$$

and since d axis of reference frame is aligned to grid voltage, accordingly $e_q = 0$, reactive power depends on the quadrature component of current (i_q)

$$Q = -\frac{3}{2} e_d i_q \tag{5.8}$$

Unity power factor condition (Q=0) is satisfied by setting the quadrature component of current zero. Average large signal model can be modified again under

steady state condition, unity power factor, and synchronous frame orientation using $e_q = 0, i_q = 0, \frac{di_q}{dt} = \frac{di_d}{dt} = 0$.

$$e_d = u_d - \underbrace{\omega_s L_g i_q}_{0} + Ri_d \quad \rightarrow \quad u_d = e_d - Ri_d \tag{5.9}$$

$$e_q = u_q + \omega_s L_g i_d + \underbrace{Ri_q}_{0} = 0 \quad \rightarrow \quad u_q = -\omega_s L_g i_d \tag{5.10}$$

$$C\frac{dV_{DC}}{dt} = Ki_d + \underbrace{d_q i_q}_{0} - \frac{V_{DC}}{R_L} \quad \rightarrow \quad \frac{dV_{DC}}{dt} = \frac{K}{C} i_d - \frac{V_{DC}}{R_L} \tag{5.11}$$

where $u_d = d_d V_{DC}$, $u_q = d_q V_{DC}$, and K is power conversion factor from 3 phase to 2 phase frame. From power invariance, $K = 1/\sqrt{3}$. For realizing control objective, since it is useful and convenient naturally for power converters, nonlinear variable structure system (VSS) control, sliding mode control, is used [12]. If dc output voltage error is written as

$$e = V_{DC} - V_{DC}^{ref} \tag{5.12}$$

where V_{DC} is measured and V_{DC}^{ref} is desired voltage, then sliding surface in sliding mode is defined as following

$$s = \dot{e} + De \tag{5.13}$$

where *D* is positive definite controller gain scalar. Inserting equation 5.13 into 5.14,

$$s = \dot{V}_{DC} - \dot{V}_{DC}^{ref} + D\left(V_{DC} - V_{DC}^{ref}\right) \tag{5.14}$$

The equivalent control is obtained using equation 5.11,

$$\dot{V}_{DC} = \dot{V}_{DC}^{ref} - D\left(V_{DC} - V_{DC}^{ref}\right) = \frac{1}{\sqrt{3}C} i_{deq} - \frac{V_{DC}}{R_L}$$

$$i_{deq} = \sqrt{3}\left(\frac{V_{DC}}{R_L} + C\left(\dot{V}_{DC}^{ref} + D\left(V_{DC}^{ref} - V_{DC}\right)\right)\right) \tag{5.15}$$

The block representation of the controller is depicted in Figure 5.6.

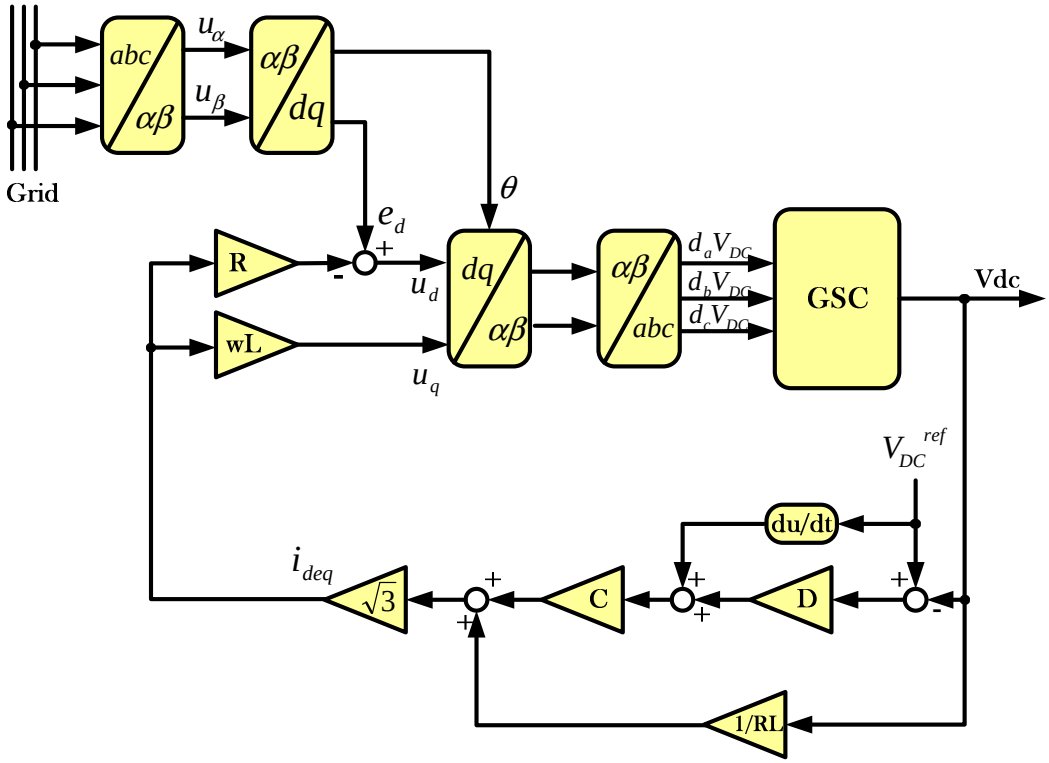

Figure 5.6. Block representation of GSC controller

5.2 Simulation Results

Unity power factor and reference voltage tracking are performed by the sliding mode control in grid side orientation. The values of grid side converter circuit parameters and controller gain are given in Table 5.1 [13].

Table 5.1. GSC simulation parameters

		Value	*Unit*
C	:	820	uF
R	:	0,15	ohm
Rload	:	182	ohm
D	:	200	

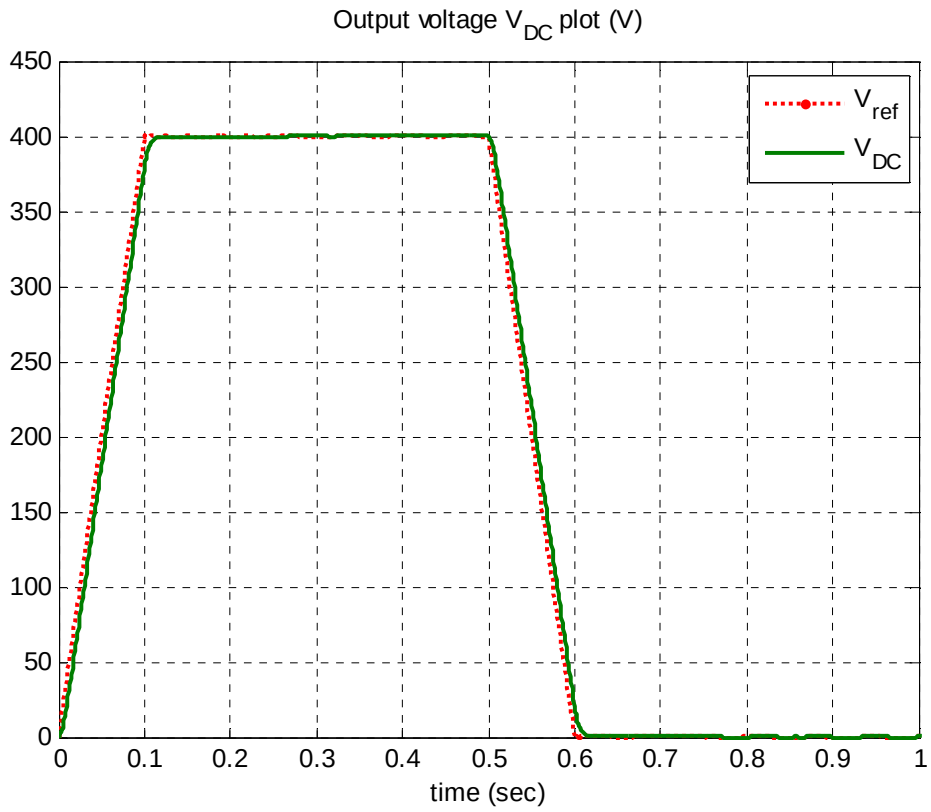

Figure 5.7. Reference voltage tracking performance of GSC

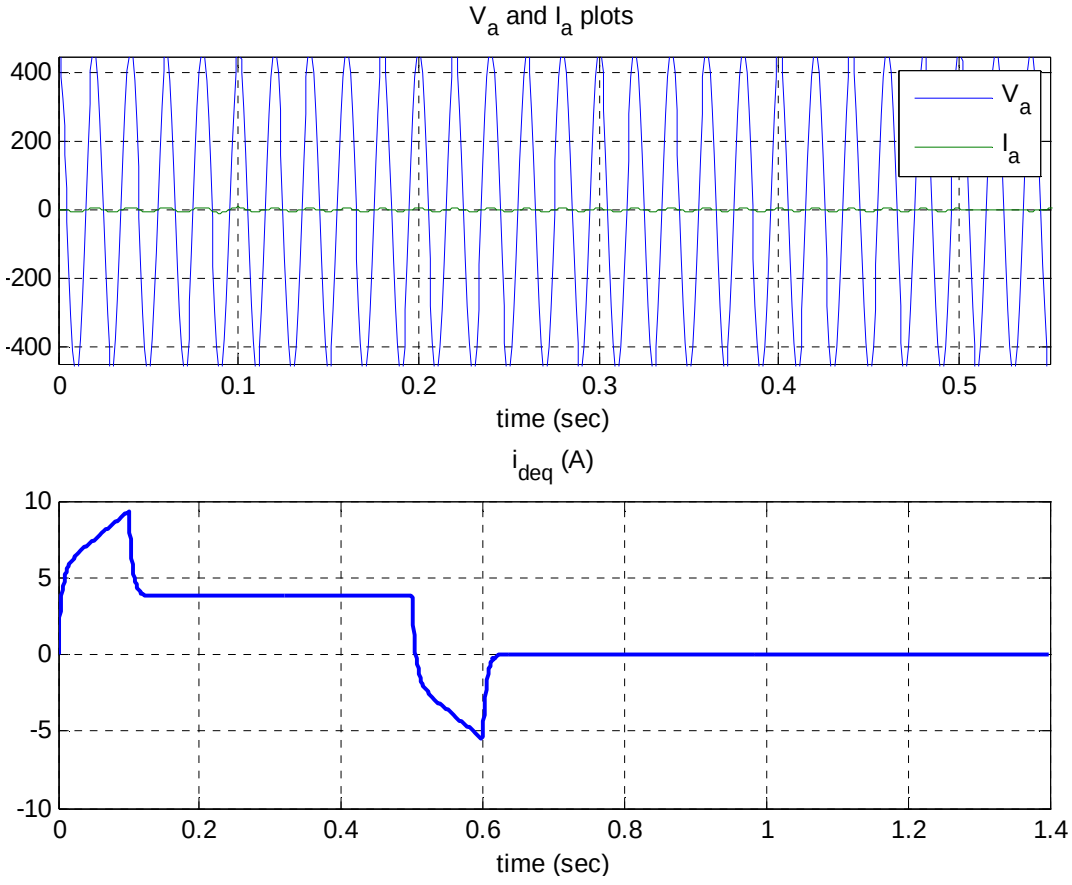

Figure 5.8. Unity power factor and equivalent control plots

As seen from simulation results, Figure 5.7 and Figure 5.8, the desired voltage is tracked under varying reference. One phase of grid voltage and corresponding current have the same phase so unity power is satisfied by equivalent control.

6 REFERENCES

[1] REN21 Secretariat, “Renewables Global Status Report 2006 update”

[2] “Renewable Energy”, http://en.wikipedia.org/wiki/Renewable_energy

[3] R. Datta, V. T. Ranganathan, “Variable-Speed Wind Power Generation Using Doubly Fed Wound Rotor Induction Machine-A Comparison with Alternative Schemes ”, *IEEE Transactions on Energy Conversion*, Vol.17, No.3, September 2002

[4] A. Petersson, “Analysis, Modelling and Control of Doubly-Fed Induction Generators for Wind Turbines”, Phd Thesis, Chalmers University of Technology

[5] S. Muller, M. Deicke, R. W. De Doncker, “Adjustable Speed Generators for Wind Turbines based on doubly-fed Induction Machines and 4-Quadrant IGBT Converters Linked to the Rotor ”, *Industry Applications Conference*, Vol.4, 2000

[6] W. Leonhard, “Control of Electrical Drives”, Springer Verlag, Berlin, 1985

[7] N. P. Quang, A. Dittrich, A. Thieme, “Doubly-fed induction machine as generator: control algorithms with decoupling of torque and power factor”, *IEEE Industry Applications Magazine*, May|June 2002

[8] M. Ünel, EE578 - Nonlinear Control Systems Lecture Notes, Sabanci University

[9] Marquez J. Horacio, “Nonlinear Control Systems: Analysis and Design”, John Wiley & Sons, 2003

[10] S. Katsura, Y. Matsumoto, K. Ohnishi, “Analysis and Experimental Validation of Force Bandwidth for Force Control”, *IEEE Transactions on Industrial Electronics*, Vol.53, No.3, June 2006

[11] S. Peresada, A. Tilli, A. Tonielli, “Power Control of a Doubly fed Induction Machine via Output Feedback”, *Control Engineering Practice* 12 (2004) 41-57

[12] K. Jezernik, D. Rutar, M. Milanovic, “Nonlinear voltage control of unity power factor boost converter”, *IEEE International Symposium on Industrial Electronics*, 1993

[13] V. Utkin, J. Guldner, J. Shi, “Sliding Mode Control in Electromechanical Systems”, Taylor & Francis, 1999